HHS Public Access

Author manuscript

ACS Infect Dis. Author manuscript; available in PMC 2022 November 28.

Published in final edited form as:

ACS Infect Dis. 2021 December 10; 7(12): 3125–3160. doi:10.1021/acsinfecdis.1c00465.

Recent Advances in the Evaluation of Antimicrobial Materials for Resolution of Orthopedic Implant-Associated Infections *In Vivo*

Erika L. Cyphert,
Department of Biomedical Engineering, Case Western Reserve University, Cleveland, Ohio 44106, United States

Ningjing Zhang,
Department of Biomedical Engineering, Case Western Reserve University, Cleveland, Ohio 44106, United States

Greg D. Learn,
Department of Biomedical Engineering, Case Western Reserve University, Cleveland, Ohio 44106, United States

Christopher J. Hernandez,
Sibley School of Mechanical and Aerospace Engineering, Cornell University, Ithaca, New York 14853, United States; Hospital for Special Surgery, New York, New York 10021, United States

Horst A. von Recum
Department of Biomedical Engineering, Case Western Reserve University, Cleveland, Ohio 44106, United States

Abstract

While orthopedic implant-associated infections are rare, revision surgeries resulting from infections incur considerable healthcare costs and represent a substantial research area clinically, in academia, and in industry. In recent years, there have been numerous advances in the development of antimicrobial strategies for the prevention and treatment of orthopedic implant-associated infections which offer promise to improve the limitations of existing delivery systems through local and controlled release of antimicrobial agents. Prior to translation to *in vivo* orthopedic implant-associated infection models, the properties (*e.g.*, degradation, antimicrobial activity, biocompatibility) of the antimicrobial materials can be evaluated in subcutaneous implant *in vivo* models. The antimicrobial materials are then incorporated into *in vivo* implant models to evaluate the efficacy of using the material to prevent or treat implant-associated infections. Recent technological advances such as 3D-printing, bacterial genomic sequencing, and real-time *in vivo* imaging of infection and inflammation have contributed to the development of preclinical implant-associated infection models that more effectively recapitulate the clinical presentation of infections and improve the evaluation of antimicrobial materials. This Review highlights the advantages and limitations of antimicrobial materials used in conjunction with orthopedic implants

Corresponding Author: Horst A. von Recum – Department of Biomedical Engineering, Case Western Reserve University, Cleveland, Ohio 44106, United States; Phone: (216) 368-5513; horst.vonrecum@case.edu; Fax: (216) 368-4969.

Complete contact information is available at: https://pubs.acs.org/10.1021/acsinfecdis.1c00465

The authors declare no competing financial interest.

for the prevention and treatment of orthopedic implant-associated infections and discusses how these materials are evaluated in preclinical *in vivo* models. This analysis serves as a resource for biomaterial researchers in the selection of an appropriate orthopedic implant-associated infection preclinical model to evaluate novel antimicrobial materials.

Graphical Abstract

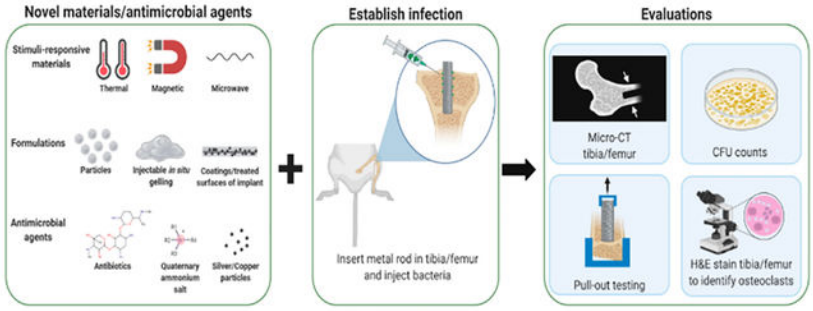

Keywords

Periprosthetic joint infection; Antibiotic; Implant; Drug delivery; In vivo

1. INTRODUCTION

Each year, >1.35 million primary arthroplasties, including >750 000 knee, >500 000 hip, and >100 000 shoulder prostheses, are performed in the United States, with procedure volumes for each of the mentioned subtypes increasing steadily year over year.[1,2] While implant-associated orthopedic infections occur in approximately 1–3% of primary arthroplasty patients, clearance of infections is nontrivial.[3] For example, patients may be subjected to prolonged antibiotic therapy, repetitive revision surgeries resulting in functional impairment, and the possibility of permanent handicap (*e.g.*, amputation).[3] Infection recurrence following revision surgeries occurs in 9–50% of patients, depending upon the type of bacteria involved, if the infection is acute or chronic, and the type of revision surgery (*e.g.*, one- versus two-stage revision, irrigation and debridement with implant retention).[4–7] Due to the rising age and longevity of the general population, the number of implant-associated infection revision procedures has been projected to increase by 43–182% from 2014 to 2030.[8] Implant-associated infections also pose a substantial socioeconomic burden, costing the healthcare system an additional ~$13 000 per patient.[9]

Implant-associated orthopedic infections can arise through several means pre- and postoperatively. For example, these infections can be initially acquired through mechanisms such as a breach of sterility during surgery (*i.e.*, surgical site infections), acute trauma (*i.e.*, open fractures),[10,11] hematogenous seeding,[12–14] or postsurgical infiltration of skin micro-flora.[15] An individual patient's risk of developing an implant-associated orthopedic infection can be exacerbated by underlying comorbidities, such as obesity or diabetes,[3,16,17] or by failure to observe proper wound care practices during the postoperative period.[15]

Both biodegradable and nondegradable biomaterials used in orthopedic implants (*e.g.*, metals, ceramics, polymers, *etc.*) have the potential to serve as a nidus for infection and bacterial attachment if the surgical site is infiltrated with bacteria.[18] When implanted materials are infected, the typical course of treatment involves determining the susceptibilities of the causative pathogen(s), perioperative systemic antibiotics, and surgical debridement and removal and replacement of nondegradable devices.[19] However, when biomaterials are effectively designed and engineered with antimicrobial properties, they can be applied to manage or treat implant-associated infections locally. Specifically, biomaterials have historically played a pivotal role in the prevention and treatment of implant-associated orthopedic infections. Since 1972, antibiotics have been directly incorporated into poly(methyl methacrylate) (PMMA) bone cement as a measure against orthopedic implant-associated infections. Antibiotic-laden PMMA thereby provides a dual functionality, mechanical stability (*e.g.*, fixing a prosthesis or serving as a temporary spacer) and antimicrobial activity.[20] Nevertheless, incorporation of antibiotics into PMMA bone cement, for example, results in insufficient elution of the drug to effectively maintain therapeutic concentrations necessary to eradicate infections.[21,22] Consequently, there has been growing interest to develop materials that provide a more controlled and consistent antimicrobial activity for orthopedic implant applications. Materials that have been recently developed for prevention and mitigation of orthopedic implant infections include stimuli-responsive (*e.g.*, to temperature, electrical/magnetic fields, microwaves, *etc.*) and nanocomposite materials.[23–30]

While many of the antimicrobial materials have shown promise in initial *in vitro* studies, translating these systems to clinically relevant orthopedic animal models presents several challenges. There are species-specific differences in the manifestation of bacterial infections in animal models as well differences in bacterial infections between animal models and humans.[31] Additionally, in clinical practice, there are patient comorbidities that can increase the risk of developing implant-associated infections (*e.g.*, diabetes, obesity, *etc.*), and due to the difficulty of recapitulating these comorbidities in animal models these factors have only recently been explored in preclinical models.[32,33] Technological advancements (*e.g.*, 3D-printing, bacterial genomic sequencing, *etc.*[33,34]) have enabled the development of more clinically relevant and reproducible *in vivo* models that may facilitate and improve understanding of the development and treatment of implant-associated infections moving forward. Furthermore, advances in real-time *in vivo* imaging modalities (*e.g.*, positron emission tomography (PET), fluorescence) and radioactive tracers and probes offer the potential to monitor the efficacy of antimicrobial orthopedic materials and progression of infection and inflammation noninvasively.[35–37]

This Review highlights the advantages and limitations of antimicrobial materials used in conjunction with orthopedic implants for implant-associated infection applications (section 3) and how these materials are evaluated in preclinical *in vivo* models for the prevention or treatment of infection (sections 4 and 5). Our analysis is intended to serve as a resource to help guide biomaterials researchers in the selection of an appropriate implant-associated infection preclinical model for evaluation of novel antimicrobial materials.

2. METHODS

To construct this analysis, a literature search was performed in PubMed with the following keywords (July 2021): “orthopedic implant infection model” (1050 results), “orthopedic implant infection animal model” (401 results), “materials prevent orthopedic implant infection” (616 results), and “materials treat orthopedic implant infection” (1321 results). The results were screened, and the biomaterials and preclinical *in vivo* models highlighted in this Review were selected based upon their publication date (within the past decade), if they developed a material to address implant-associated infections ($n = 45$), and if they either established a novel orthopedic implant-associated infection model ($n = 28$) or used an orthopedic implant-associated infection model to evaluate the ability of biomaterials to prevent or treat infection ($n = 88$).

3. ADVANTAGES AND LIMITATIONS OF ANTIMICROBIAL BIOMATERIALS USED FOR PREVENTING/TREATING IMPLANT-ASSOCIATED INFECTIONS

Antimicrobial materials surveyed in this Review comprise those that combat infections directly and indirectly. Specifically, materials that exhibit bactericidal or bacteriostatic activity through the release of antimicrobial agents and materials that repel the adherence of bacteria (*e.g.*, nanotopography, surface treatments) are included.[38–41] This Review primarily focuses on the material-level properties of the antimicrobial biomaterials used in conjunction with orthopedic implants and does not consider the design and properties of the orthopedic implant device/component itself (*e.g.*, Kirschner wires, screws, *etc.*) unless it has been modified to exhibit antimicrobial activity (*e.g.*, nanotopography, surface coating, *etc.*). For the context of this Review, an orthopedic antimicrobial biomaterial is defined as a material that has been designed to work in conjunction with permanent orthopedic implants to provide localized antimicrobial therapy and support the function of the implant (*e.g.*, materials with antimicrobial activity alone and those with antimicrobial activity and osteoconductive properties). Tables 1–4 highlight the advantages and limitations of a selection of antimicrobial biomaterials from the past decade that have been developed to address orthopedic implant-associated infections.

3.1. Metals.

A variety of metals and alloys have been used in preclinical models for the prevention and treatment of orthopedic implant-associated infections (Table 1). While many of the metals frequently utilized in orthopedic implants are not inherently antimicrobial (*e.g.*, titanium and titanium alloys (Ti6Al4V),[42–44] cobalt–chromium–molybdenum (Co–Cr–Mo alloys),[45] stainless steel (316L),[46–48] *etc.*), surface modifications (*e.g.*, atomic layer and plasma electro-deposition[49–53]) can be used to coat the implant with antimicrobial metal nanoparticles (*e.g.*, silver,[52–54] copper,[52,55,56] zinc,[53,57] magnesium,[58,59] gold, *etc.*).

Due to their intrinsic antimicrobial activity, coatings with silver, gold, copper, zinc, or magnesium are particularly advantageous because they can provide long-term broad-spectrum antimicrobial activity without the use of antibiotics (*i.e.*, offer a decreased risk of stimulating bacterial resistance[53,60,61]) and are gradually released over a prolonged

period (30 days).[62] Generally, smaller nanoparticles (~10–15 nm diameter) have improved biocompatibility, can penetrate bacterial cells, and have more potent antimicrobial activity than that of larger nanoparticles.[63,64] The geometry of nanoparticles also influences their antimicrobial activity (*e.g.*, nanoparticles with sharp edges have increased antimicrobial activity).[65]

There are several proposed mechanisms of action for the antimicrobial activity of metallic nanoparticles including production of intracellular reactive oxygen species and hydrogen peroxide damaging bacterial proteins, damage to the bacterial cell membrane via electrostatic penetration (*e.g.*, cations bind to anionic lipopolysaccharides in membrane of bacteria cell), and prevention of the replication of bacterial DNA.[66,67] The amount of reactive oxygen species produced, for example, can be used to evaluate the antimicrobial activity of metallic nanoparticle implant coatings.[52,68] Alternatively, antimicrobial properties can be imparted to certain metals, such as titanium, when they are exposed to aerobic environments oxidizing the surface (TiO_2).[69,70] The surface of metallic implants can also be modified to have a nanotopography architecture.[38–40] A rough textured implant surface increases the surface area that the bacterial cells are exposed to, enhancing antimicrobial activity.[38,39] Certain surface modifications to metals including plasma electrolytic oxidation[53] and phosphorus doping[40] have been shown to enhance osseointegration of the antimicrobial materials. Plasma electrolytic oxidation is attractive due to its ease of use, high deposition rate,[71] and ability to create multifunctional surfaces (*e.g.*, antimicrobial and osteoconductive).[53] Phosphorus doping provides a bottle-shaped nanostructure that assists in osseointegration.[40]

Nevertheless, antimicrobial metallic materials have several limitations. Specifically, they can release metallic ions and particles that can enter the lymphatic and circulatory system and cause damage when they accumulate in tissues (*e.g.*, genotoxicity)[72–77] or are excreted (*e.g.*, nephrotoxicity).[78,79] Ions from Co–Cr–Mo alloys are particularly problematic due to their carcinogenicity.[80] Additionally, metallic ions generally have a lack of specificity and have been shown to exhibit cytotoxicity to eukaryotic cells in high concentrations.[53] Therefore, in some cases, different metallic nanoparticles in the coating (*e.g.*, silver and zinc, *etc.*) have been combined to offer comparable antimicrobial activity to individual metals while reducing cytotoxicity by decreasing the concentration of nanoparticles of a single composition.[53] Furthermore, since many metallic antimicrobial materials are nondegradable, they have the potential to harbor bacterial biofilms (*i.e.*, dense cluster of sessile bacteria encapsulated in extracellular polymeric substance with protein, lipids, and teichoic acids[81]), which typically result in invasive debridement, removal, and replacement of the implant.

3.2. Polymers.

Natural and synthetic polymeric materials have been developed to prevent and treat orthopedic implant-associated infections (Table 2). While a number of polymeric materials have intrinsic antimicrobial activity (*e.g.*, silicone nanotopography that can repel bacteria,[41,82] chitosan,[83] hyaluronic acid,[23,84,85] *etc.*), it is often necessary to incorporate antibiotics into polymeric materials to impart antimicrobial activity.[23,24,83,86–105] The rate of enzymatic/hydrolytic degradation of biodegradable polymers such as chitosan,[24,83,99]

hyaluronic acid,[23,85] alginate,[85,105] poly(lactic acid) derivatives (*e.g.*, poly[L-lactic] acid, poly[D,L-lactide-*co*-lactide], poly[D-L-lactide]),[87–89,94–96] polycaprolactone,[87,98,100] and poly(lactic-*co*-glycolic acid) (PLGA)[35,98,100,101,104,106] dictates the rate of antibiotic release from the implanted material and subsequent duration of antimicrobial activity. An advantage of biodegradable polymeric materials is that their rate of degradation can be tailored through several means including their molecular weight and degree of crystallinity.[107] Specifically, for chitosan, several factors including the degree of deacetylation and molecular weight can influence the rate of degradation.[108] If chitosan has a higher degree of deacetylation (processed in alkaline conditions), it will have a greater hydrophilicity and have an increased degradation rate.[108] The degradation rate and hydrophilicity of hyaluronic acid can be influenced by the chemistry of the cross-linking agent used, for example,[109] whereas the degradation rate of hydrolytically cleavable copolymers, such as PLGA, for example, can be increased by incorporating a greater fraction of the relatively hydrophilic component poly(glycolic acid) at the molecular level.[110] Additionally, naturally derived polymers (*e.g.*, chitosan, hyaluronic acid, and alginate) exhibit excellent biocompatibility.[111]

Nondegradable polymeric materials such as poly(ether ether ketone),[97,112–119] poly(ethylene glycol) (PEG),[90–92,98,104,120] poly(ethyleneimine),[121,122] cyclodextrin,[29,123–125] poly(methyl methacrylate) (PMMA),[29,34,86,118,119,123–134] polyethylene terephthalate,[37,87] silicone,[41,135] and polyesters[87,93] have the potential to serve as long-term antimicrobial materials. Since the release of antibiotics from nondegradable materials is not associated with the rate of degradation of the material, these materials primarily rely on diffusion and affinity-based interactions to dictate the release kinetics of antibiotics. Poly(ethyleneimine) is a versatile polymer that has been used in layer-by-layer coatings of orthopedic implants to regulate drug release,[121] and in its quaternized form it is intrinsically antimicrobial.[122] Nevertheless, it is important to consider that poly(ethyleneimine) has been shown to exhibit cytotoxic effects and the mechanisms of cytotoxicity are still being investigated.[136] Poly(ether ether ketone) and PMMA are particularly amenable for orthopedic load-bearing applications due to their mechanical properties (ability to resist wear following long-term cyclical loading).[137,138] In terms of prevention of implant-associated infections, degradable antimicrobial polymers are advantageous relative to nondegradable antimicrobial polymers. Specifically, if a bacterial biofilm is to form on a nondegradable material, complete eradication of the infection often requires a full surgical debridement and replacement[139] and biodegradable materials have been shown to have a decreased risk of developing bacterial biofilms (*e.g.*, decreased surface area for attachment during degradation, *etc.*).[139] However, there are some nondegradable materials such as insoluble cross-linked cyclodextrin that has been shown to retain its ability to be repeatedly filled with antibiotics even in the presence of a bacterial biofilm.[140]

Several polymeric antimicrobial biomaterials offer the advantage of stimuli-responsive properties that enable control of gelling and release of antibiotics. For example, chitosan functionalized materials have been formulated to be thermosensitive and gel following injection, enabling minimally invasive application.[23,24] Additionally, polymers including PEG, PLGA, and alginate have been formulated to gel *in situ*.[85,104,105]

3.3. Ceramics.

A range of ceramic materials have been used in preclinical orthopedic antimicrobial applications including calcium sulfate,[28,141–145] hydroxyapatite,[144,146–148] β-tricalcium phosphate,[145] zirconium nitride,[149] borate bioactive glass,[30] and calcium phosphate[113,150] (Table 3). Several ceramics are intrinsically antimicrobial, such as calcium phosphate and bioactive glass;[151,152] however, for orthopedic implant infection applications, ceramics often incorporate antibiotics. For degradable ceramic materials (*e.g.*, calcium phosphate, calcium sulfate, hydroxyapatite, *etc.*), the rate of antibiotic release is strongly dependent upon the rate of degradation. Degradation of calcium phosphate materials including hydroxyapatite and β-tricalcium phosphate is mediated by physical, chemical, and biological factors including crystallinity, porosity, pH, and ionic substitutions.[153] An advantage of these materials is that their physical properties can be tailored to obtain the desired degradation and subsequent release kinetics of incorporated antibiotics.[153,154] Recently an injectable formulation of bioactive glass has been developed to enable noninvasive application of the antibiotic carrier for treatment of orthopedic implant infections.[30] An advantage of ceramic orthopedic antimicrobial materials is that they often have crystalline structures that mimic the structure of bone and exhibit excellent osteoconductive properties.[151,155] Calcium phosphate, for example, releases calcium and phosphate ions that bind collagen and promote bone in-growth to the implant.[156] Despite their excellent osteoconductive properties and tunable drug release, many ceramic antimicrobial materials are not amenable for load-bearing orthopedic applications. For example, bioactive glass, hydroxyapatite, and calcium phosphate can be brittle.[151]

3.4. Composites.

Antimicrobial orthopedic composite materials are composed of a combination of metal, polymer, and ceramic materials (Table 4). Ceramics including zirconium nitride,[149] hydroxyapatite,[146–148] and calcium phosphate[157] have been used as coatings on titanium, titanium alloy, and cobalt–chromium–molybdenum implants in implant-associated infection models. An advantage of composite materials is that they can incorporate the beneficial properties of both materials to create a dual-functioning system. For example, when osteoconductive ceramic materials such as hydroxyapatite are combined with intrinsically antimicrobial silver, the composite can simultaneously provide antimicrobial activity while promoting osseointegration of the implant.[146–148,157]

An advantage of composite materials is that they can be designed to address drug delivery limitations of individual materials. Specifically, antibiotics are generally incorporated directly into cement materials (*e.g.*, PMMA bone cement, calcium sulfate, borate bioglass) to impart antimicrobial activity.[28–30,123–125] Nevertheless, antibiotic release kinetics from nondegradable cements (*e.g.*, PMMA) are suboptimal as a small amount of antibiotic is only released from the surface of the PMMA (~10% of incorporated drug) and the rest remains entrapped permanently.[158] Antibiotic release from degradable cements (*e.g.*, calcium sulfate and borate bioglass) is dependent upon the rate of degradation of the material.[30] To enable a more controlled release of antibiotics from cements, polymers such as cyclodextrin[29,123–125] and cationic liposomes[28] have been incorporated. Specifically, insoluble antibiotic-filled cyclodextrin microparticles have been incorporated into PMMA bone cement and have been

shown to enable a more prolonged and consistent release of antibiotics at therapeutically relevant levels.[29,123–125] Cationic liposomes have been incorporated into calcium sulfate to locally increase antibiotic concentration at the implant infection site.[28] Nevertheless, depending upon their composition, composite materials may still have the limitations of individual materials (*e.g.*, leach cytotoxic metallic ions, risk for formation of bacterial biofilms on nondegradable materials).

4. EVALUATING THE EFFICACY OF BIOMATERIALS TO PREVENT/TREAT IMPLANT-ASSOCIATED INFECTIONS *IN VIVO*

4.1. Considerations in Establishing Clinically Relevant Preclinical Implant-Associated Infection Models.

When establishing an orthopedic implant-associated infection *in vivo*, there are several factors that must be considered. For example, the inoculum used to generate the infection should be relevant to the animal species and region of the body, and this must be determined through a series of preliminary studies. An excessively large inoculum can cause sepsis and death while an insufficient inoculum will quickly be cleared.[34,163,164] The duration of time following the inoculation of the pathogen in which the infection is established in the model must also be considered since this is dependent upon the species used in the model and differs from clinical presentation.[31] Additionally, the virulence of the bacterial strain used in the model and the culture conditions (*i.e.*, log phase versus stationary phase growth) impact the concentration of the inoculum required to establish an infection.[165] Furthermore, the aim of the *in vivo* model (*i.e.*, acute versus chronic infection) dictates the selection of the bacterial species used. Specifically, if the model is studying acute infection, bacteria with a high virulence will be used (*e.g.*, *S. aureus*), whereas if the model is studying chronic infection low virulence bacteria will be used (*e.g.*, coagulase-negative staphylococci).[166] It is also important to consider that bone remodeling kinetics are dependent upon the species used in the *in vivo* model and that these kinetics differ from those observed in humans.[167] As a result, the time course for acute and chronic implant-associated infections (*i.e.*, duration of experimental study) varies across animal species and humans. To improve the clinical relevancy of the infection *in vivo*, it is also critical that the location and placement of the implanted material allow for weight-bearing locomotion.[168]

Table 5 provides a summary of *in vivo* models from the past decade that have been used to establish and study implant-associated infections in a variety of species (*e.g.*, zebrafish,[169] mice,[32,33,115,163,170–175] rats,[12,36,116,117,128,176–180] rabbits,[34,134,181–183] pigs,[184,185] *etc.*). Generally, these models involve placing either a stainless steel, titanium, or titanium–aluminum (Ti6Al4V) alloy implant in the animal's tibia (proximal tibia)[173] or femur (lateral femoral condyle).[179] Once implanted, a bacterial culture is inoculated into the intra-articular space near the implant.[173] Implant-associated infection models have been established using a range of bacteria including *Staphylococcus aureus* and methicillin-resistant *S. aureus* (MRSA),[32–34,36,115,117,128,134,169–182,184,185] *Staphylococcus epidermidis*,[116] *Escherichia coli*,[163,180] *Pseudomonas aeruginosa*,[163] *Propionibacterium acnes*,[116,183] and *Streptococcus agalactiae*.[172] Bioluminescent strains of bacteria (*e.g.*, *S. aureus*, *E. coli*) are frequently used

to enable *in vivo* tracking and imaging of the extent and evolution of the infection over time.[33,87,90–92,97,118,119,126,127,163,173–175,179,186–190]

Once the infection is established, a series of evaluations are carried out to analyze the extent of the implant-associated infection pathogenesis. Clinically, in periprosthetic joint infections (PJIs), for example, a variety of analyses have been employed.[191–193] For example, measurement of erythrocyte sedimentation rate, serum C-reactive protein, white blood cell count in synovial fluid, and radiographic imaging have all been utilized as metrics for implant-associated infections clinically,[191,194,195] and many of these analyses translate to *in vivo* models. Over the duration of a study, blood is collected to monitor the evolution of the infection through erythrocyte sedimentation rate, serum amyloid A (a factor that, in the mouse, is more sensitive than serum C-reactive protein),[33,173] white blood cell count, and presence of inflammatory cells.[32,34,179,185] To measure and track the extent of the infection during and at the end of the study, *in vivo* bioluminescence imaging (BLI) of bacteria and colony forming unit (CFU) counts in excised bone and synovial tissue and on removed implants have been analyzed.[12,32,33,36,115–117,128,134,163,170–179,182,183,185] Histology (*e.g.*, hematoxylin and eosin, Gram stain, tartrate-resistant acid phosphatase (TRAP)) is performed on excised bone and synovial tissue to supplement CFU counts and to identify osteoclasts.[12,32,36,115,117,128,163,169–172,174,176–179,182,183,185] Scanning electron microscopy (SEM) and crystal violet staining are used to further examine the architecture and presence of bacterial biofilm on the excised implant.[32,170,173,175,181] Radioactive tracers (*e.g.*, ^{18}F-fluoro-deoxy-glucose, ^{68}Ga-citrate-chloride) are used in combination with positron emission tomography (PET) to enable visualization of inflammation at the implant infection site.[36,163] A combination of X-ray and microcomputed tomography (micro-CT) imaging and gait analysis studies are applied to identify possible osteolytic regions surrounding the implant and to determine if the infection has a deleterious impact on the ambulation of the animals.[12,32,33,116,117,128,134,163,170–174,176–179,181,182,184,185]

Models highlighted in Table 5 have a variety of goals including those that strive to study implant-associated bacterial biofilms,[170,175] establish new methodologies for improving *in vivo* imaging of implant-associated infections,[36,116] evaluate hematogenous implant-associated infections,[12,185] and study a range of aerobic and anaerobic pathogens (*e.g.*, *S. agalactiae*, *P. acnes*, *E. coli*, *P. aeruginosa*, *etc.*).[163,172,183]

4.2. Considerations in Evaluating Activity of Antimicrobial Materials in Preclinical Models.

Prior to incorporating antimicrobial orthopedic biomaterials in implant-associated infection *in vivo* models, the properties of the materials can be first evaluated in *in vivo* models without tibial or femoral implants (*e.g.*, materials can be placed into dorsal subcutaneous pouches).[37,41,59,83,87,135,144,148,161] Table 6 provides a summary of preclinical *in vivo* models that have been used within the past decade to evaluate antimicrobial activity, drug release kinetics, and degradation of antimicrobial orthopedic materials.

To detect the presence and concentration of eluted antibiotics from the implanted biomaterial, blood can be collected both throughout the experiment and terminally in conjunction with hard and soft tissues surrounding the material.[83,142–144,161,196,197] The

antibiotic can then be extracted from the serum and tissues, and high performance liquid chromatography (HPLC) and liquid chromatography–mass spectrometry (LC-MS) can be used to quantify the systemic and local concentration of the antibiotics.[83,142–144,161,196,197] Following euthanasia, residual drug remaining entrapped in the implanted material can be extracted and evaluated for its concentration and antimicrobial activity in the zone of inhibition assays.[87] Alternatively, the antimicrobial activity of the material can be evaluated indirectly through the quantification of the extent of infection remaining throughout the study. Specifically, techniques such as *in vivo* BLI can be used in conjunction with bacteria that have been genetically modified to express the lux operon (*e.g.*, Xen strains) such that the extent of the infection can be imaged in real time.[59,87,198] Additionally, the extent of infection remaining can be evaluated at the termination of the study through removal of the material and SEM imaging of the morphology of the bacterial biofilm and CFU counts of adherent bacteria.[37,40,41,59,87,120,135,148,197] To evaluate the degradation of implanted materials *in vivo*, the material can be explanted with surrounding subcutaneous tissue at intermediate time points throughout the study and characterized for its morphology using SEM, molecular weight using gel permeation chromatography, glass transition temperature using differential scanning calorimetry, and residual weight.[83,199]

4.3. Considerations in Evaluating Mechanical Strength of Antimicrobial Materials in *In Vivo* Models.

When orthopedic antimicrobial materials are used in load-bearing applications (*e.g.*, antibiotic-laden PMMA bone cement implanted around arthroplasty components), it is critical that the system is mechanically robust and integrates with native bone tissue.[200] While American Society for Testing and Materials (ASTM) and International Organization for Standardization (ISO) standards have been well-established for evaluating compressive strength, 3- and 4-point bending strength, impact and fatigue strength, and intrusion of PMMA bone cement,[201,202] there is currently no standardized evaluation protocol for interfacial shear strength of the PMMA bone cement/bone interface. Since interfacial shear strength is a metric reflective of the ability of PMMA bone cement to integrate with trabecular bone and poor interlock can result in failure of the material, it is a crucial factor to consider.[203] Several groups have developed *in vivo*/*ex vivo* push-out and pull-out tests to quantify the interfacial shear strength of PMMA bone cement and other composites, nevertheless, there are inherent challenges in the standardization of these testing methods.[204–210] In both preclinical and clinical settings, age, sex, size and type of defect, the composition, method of preparing, and amount of PMMA bone cement, and the setting time, temperature, humidity, and moisture/fluid composition prior to testing are all factors which must be considered to standardize interfacial shear strength testing methodologies.[211] In general, it has been historically challenging to compare results of the mechanical properties of PMMA bone cement across studies due to a lack of standardization and detail of storage and preparation conditions of the samples.[211]

Pull-out testing is frequently used in implant-associated infection *in vivo* models where the metallic or polymeric implant integrates with native bone for a period, dependent upon the animal species and age and the rate of bone remodeling.[212] Upon completion of the study, tibial/femoral tissue is excised and fixed in PMMA bone cement and uniaxial tensile loading

is used to determine the force required to remove the osseointegrated implant from the bone.[205,213–215] Push-out testing serves an analogous function to pull-out testing. Despite the similar goals of pull- and push-out studies it is challenging to compare interfacial shear strength values across studies. Specifically, a wide range of loading rates have been used in pull- and push-out testing, depending upon the species, from 0.0083 to 0.5 mm/s, which can influence the resultant interfacial pull-out strength.[206,207,213–216] Calculation of interfacial shear strength from raw load–displacement plots is also highly variable. For example, some studies define interfacial shear strength as the peak force on the load–displacement plots when the implant is fully removed from the bone or the bone is fractured, while others interpret interfacial shear strength as the force resulting when the implant is only slightly displaced in the bone.[206,213,215] Interfacial strength can also vary based upon several factors including the geometry of the bone and the implant placement within the bone (*e.g.*, contact area of trabecular versus cortical bone).[207,209] Prior studies have demonstrated the key role that bone density plays in influencing interfacial shear strength; thus, if a greater percentage of the implanted material is in contact with cortical bone relative to trabecular bone, the interfacial strength will be increased.[209] Interfacial shear strength also depends upon the type of material used in the implant, the duration that it is implanted in the animal (*in vivo* versus solely *ex vivo*), and the species and relative mobility of the animal (*i.e.*, relative mechanical loading that the implant will experience).

Nevertheless, due to the heterogeneous nature of clinical cases, for example, patients that present with comorbidities (*e.g.*, diabetes, osteoarthritis, *etc.*) that interfere with bone matrix deposition and healing, it is challenging to compare outcomes from preclinical interfacial shear strength studies to what would occur clinically and bone remodeling kinetics differ across animal species.[167,217,218] As a result, the osseointegration of the implanted biomaterial can be evaluated using histology in conjunction with biomechanical testing.[32,179,185] Infiltration of inflammatory cells (*e.g.*, macrophages, neutrophils, monocytes, foreign body giant cells, *etc.*) in tissue surrounding the implanted material is indicative of osteolysis as inflammatory cells release cytokines (*e.g.*, tumor necrosis factor-alpha (TNF-α), interleukins (IL-1, IL-6), *etc.*) that recruit osteoclasts and promote osteolysis and loss of fixation of the implant.[32,179,185,219] Additionally, radiographs and micro-CT can be used to image osteolysis.[179,185,220]

5. INCORPORATING ANTIMICROBIAL MATERIALS INTO IMPLANT-ASSOCIATED INFECTION PRECLINICAL MODELS

5.1. Preclinical Models to Evaluate Prevention of Implant-Associated Infections.

In vivo models have been established to enable evaluation of the ability of antimicrobial biomaterials to prevent orthopedic implant-associated infections in a variety of species including mice,[38,90–93,186–188,221–224] rats,[94–99,112–114,122,129,189,225–234] rabbits,[23,26,100–102,150,157,190,235–240] sheep,[103,104,241–244] and goats[130,245] (Table 7). In these models, a metallic component is placed in either the tibia or femur and the prophylactic antimicrobial material is placed at the time of bacterial inoculation to enable evaluation of the ability of the material to prevent the development of implant-associated infection. Throughout the duration of the study, the extent of infection can be monitored

through the use of *in vivo* BLI in conjunction with luminescent bacteria (*e.g.*, Xen strains).[90–93,100,186–189] The ability of the antimicrobial implant to prevent the infection can be determined via quantification of the bacteria remaining following euthanasia using CFU counts on the surface of the implant, and the morphology of bacterial biofilms can be analyzed using SE M.[23,26,38,90–100,102–104,114,129,130,150,157,188,190,216,221,222,227–234,236–244] Additionally, the concentration of antimicrobial agent (*e.g.*, antibiotics or metallic ions) used to prevent infection can be evaluated through collection of blood and soft tissues surrounding the implanted antimicrobial material. Specifically, the antibiotic and metallic ions (*e.g.*, silver, titanium) can be extracted from the serum and tissues and quantified using HPLC (for antibiotics) and inductively coupled plasma mass spectrometry (for metallic ions).[241,242,245]

Models for the prevention of implant-associated infection included in Table 7 serve a variety of functions including those that evaluate systemic delivery of drugs,[188,223] evaluate the effect of the surface properties and topography of the implant,[38,232,237] and evaluate materials that provide both antimicrobial activity and promote osseointegration[97,112,113,122,186,187,190,225,229–231,234,236,238] and those that evaluate intrinsic antimicrobial materials (*e.g.*, without antibiotics).[112,122,150,157,227,230,233,234,238,245,246]

5.2. Preclinical Models to Evaluate Treatment of Implant-Associated Infections.

Orthopedic implant-associated infection *in vivo* models that incorporate antimicrobial biomaterials have been developed to treat established infections following an initial debridement in a variety of species including mice,[118,119,126,127,247–249] rats,[25,27,85,86,105,131,250–255] rabbits,[24,28,30,35,106,132,133,235,256–258] and dogs,[259] for example (Table 8). Models that evaluate treatment of implant infections generally involve an initial implantation of a tibial or femoral implant and bacterial inoculation. Following inoculation, the implant-associated infection is allowed to develop for a period (dependent upon the species). Once the infection has been established (typically ≥ 7 days), the surgical site is debrided and an antimicrobial biomaterial is implanted. The efficacy of the antimicrobial material to treat and clear established implant-associated infections is evaluated through terminal CFU counts on implants and surrounding tissue, morphology of bacterial biofilms on implanted materials (SEM), and histology of tissue surrounding the infected implant.

Models for the treatment of orthopedic implant-associated infection included in Table 8 serve a variety of functions including those that evaluate the efficacy of antibiotic dosing regimens,[27,248–250,253,254] antibiotic-alternative agents (*e.g.*, silver),[251,252,258] cement spacers,[28,86,118,119,126,127,131–133,235,247] and injectable implants[24,30,85,105] and use novel imaging modalities to monitor the infection in real time.[35]

6. RECENT ADVANCES IN ORTHOPEDIC ANTIMICROBIAL MATERIALS AND PRECLINICAL MODELS TO IMPROVE TREATMENT AND EVALUATION OF IMPLANT-ASSOCIATED INFECTIONS *IN VIVO*

6.1. Stimuli-Responsive Antimicrobial Materials.

Over the past decade, there have been numerous advances in the development of stimuli-responsive antimicrobial orthopedic materials that respond to temperature,[23,24] magnetic fields,[25,26] microwaves,[26] and electrical fields,[27] for example. Polymer hydrogels of hyaluronic acid and chitosan have been chemically modified to induce thermoresponsive properties.[23,24] Poly(*N*-isopropylacrylamide) has been engrafted onto hyaluronic acid to develop an injectable hydrogel that shifts from a sol to gel state when it reaches body temperature due to the conformational change of the poly(*N*-isopropylacrylamide) chains as they exceed their lower critical solution temperature.[23,261] Glycerol phosphate disodium salt has been used to induce thermoresponsive properties to chitosan.[24,262] Thermoresponsive polymers have been combined with antibiotics, thereby creating a biodegradable and biocompatible delivery system that can be applied minimally invasively to treat or prevent orthopedic implant infections. The thermoresponsive systems have been shown to effectively promote bone regeneration and clear infection in preclinical models.[23,24]

Alternatively, several orthopedic antimicrobial materials have been developed that are responsive to magnetic fields and microwaves. Gelatin coated magnetite nanoparticles have been used in conjunction with an external neodymium magnet to guide the location of the injected particles to the target site (implant infection).[25] Additionally, materials that combine several stimuli (*e.g.*, magnetic field, microwaves, temperature) have been engineered to target deep tissue orthopedic implant-associated infections.[26] Magnetic iron oxide (Fe_3O_4) nanoparticles have been combined with carbon nanotubes, antibiotics, and 1-tetradecanol for a “bacterial-capturing” stimuli-responsive system.[26] Specifically, iron oxide nanoparticles and carbon nanotubes generate heat when they are exposed to high microwaveocaloric therapy and 1-tetradecanol is thermoresponsive and allows for a controlled release of the encapsulated antibiotic at the elevated temperatures.[26]

Additionally, an external treatment to titanium implants has recently been explored where a constant cathodic voltage is applied 7 days following implantation and establishment of infection.[27] This treatment has been shown to reduce bacterial adhesion to the surface of the implant by increasing the interfacial capacitance and decreasing the polarization resistance of the titanium.[263] This treatment offers promising results where an external electrical stimulation may be used to noninvasively induce antimicrobial properties to the surface of titanium implants, without the need to chemically modify the surface of the implant.

6.2. Improved Recapitulation of Clinical Orthopedic Implant-Associated Infections *In Vivo*.

Widespread adoption of emerging technologies such as 3D-printing, bacterial genomic sequencing, and microbiome profiling have contributed to the development of orthopedic implant-associated infection *in vivo* models that more effectively recapitulate the clinical

presentation of infections. Figure 1 highlights some of the recent advances in implant-associated infection *in vivo* models.

Decreasing costs of additive manufacturing over the past decade enable new implant designs that were previously impractical.[264,265] For example, 3D-printing has been used to design custom-fit orthopedic metallic *in vivo* implants in rabbits.[34,134] Micro-CT scans of the intact knee joint are used to design custom stainless steel tibial inserts.[34,134] Custom species-specific implants are particularly advantageous over implants traditionally used in preclinical models (non-species-specific) because they are more representative of clinical arthroplasties, may allow for more reproducible studies, and enable accelerated postsurgical loading of the implant to improve the evolution and treatment of implant-associated infections.[34,134] Nevertheless, the time intensive nature of custom printing implants that require initial micro-CT scans may hinder the progression of such models.

The 2018 International Consensus Meeting on Musculoskeletal Infection generated a list of "high priority" research questions related to implant-associated infections, half of which focus on modifiable patient factors.[266] Animal models represent the best way of evaluating the contributions of patient factors to infection and have previously not been the focus of preclinical orthopedic infection models. Diabetes is a known risk factor for implant-associated infections due to the patient's impaired innate immune system response and vasculopathy.[32] Establishment of an effective diabetic implant-associated infection *in vivo* model can assist in the study of the progression and treatments of implant-associated infections for patients with an underlying comorbidity.[32] More recently, the constituents of the gut microbiome have been implicated as a factor that can influence the development of implant-associated infections. Mice in which the composition of the gut microbiome had been modified throughout life were subjected to implantation of a titanium tibial component and bacterial inoculation.[33] Disruption of the gut microbiome resulted in a reduced ability to resist a small local inoculation of *S. aureus* as measured by CFU counts at the implant surface. Additionally, even when an infection was present, animals with an altered gut microbiome showed a reduced systemic response to implant-associated infection in the form of more muted changes in serum markers and immune cell populations following infection. These studies examining diabetes and the gut microbiome are just a few examples of ways in which animal models can be used to identify mechanisms linking patient factors to risk of implant-associated infection and ways of mediating that risk. Establishment of *in vivo* models that account for patient factors that more accurately portray clinical conditions can improve the evaluation of antimicrobial biomaterials in orthopedic implant-associated infection models.

6.3. Method to Assist in Standardization of *Ex Vivo* Mechanical Testing of Antimicrobial Materials.

Due to the variability of parameters used in existing pull- and push-out strength models, a standardized metric to evaluate interfacial shear strength would be desirable to ensure that antimicrobial arthroplasty materials are capable of withstanding shear forces. Ongoing work has focused on the development of a reproducible *ex vivo* push-out test method to calculate interfacial shear strength at the interface of bone and implanted PMMA bone cement. In

this model, widely available cleaned/bleached bovine femoral tissue is used and machined into wafers (~4 mm thickness) with up to eight 5/32 in. diameter holes where PMMA is embedded (Figure 2). The bone wafer containing PMMA is then subjected to push-out testing under compressive loading using a specialized jig to ensure proper alignment of the pin (1/8 in. diameter) above each PMMA implant. Interfacial shear strength is defined as the peak force on the load–displacement plot. The setup of this push-out testing *ex vivo* model is particularly advantageous because many implants can be evaluated rapidly (up to 8 per waver) and the bone wafer has a uniform geometry, is reproducible, and can be customized in terms of the number of implants per wafer. Additionally, the bone wafer can be designed for bones of other large animal species (*e.g.*, sheep). While this model may offer the possibility of assisting in the reproducibility of interfacial shear strength, it has several limitations. Specifically, the *ex vivo* model only provides basic information on the interdigitation of PMMA into excised bone and does not provide insight into the osseointegration of the PMMA upon bone remodeling *in vivo*. Additionally, this system may only be amenable for larger animal species.

6.4. Enhanced *In Vivo* Imaging of Implant-Associated Infections.

To enhance the capabilities of imaging implant-associated infections real time *in vivo*, several radioactive tracers and probes have been developed. Radioactive tracers fiuorine-18-fluoro-2-deoxy-D-glucose (^{18}F-FDG), gallium-68-labeled citrate (^{68}Ga-citrate), and gallium-68-labeled chloride (^{68}Ga-chloride) have recently been used to obtain high resolution images of orthopedic implant-associated infections[35,36] when combined with positron emission tomography and computed tomography. Both ^{18}F and ^{68}Ga have been shown to have an increased uptake at the sites of bacterial infections. While ^{18}F and ^{68}Ga have a similar uptake at bacterial infection sites, ^{18}F has been shown to have a greater uptake in healing bone relative to ^{68}Ga; therefore, recent evidence has shown that ^{68}Ga imaging may be more amenable to use in implant-associated infection studies when bone healing is involved.[36] Additionally, near-infrared fluorescent molecular probes composed of the fluorophores *H*-sulfo-cyanine5 and diaminocyanine sulfonate have been developed to enable real-time imaging of inflammation and implant-associated infections noninvasively.[37] Reactive oxygen species are associated with inflammation, and *H*-sulfo-cyanine5 fluoresces when it reacts with reactive oxygen species, thereby enabling imaging of inflammatory sites,[37] whereas nitric oxide is released at bacterial infection sites, and diaminocyanine sulfonate fluoresces when it reacts with nitric oxide.[37] Real-time monitoring of implant-associated infections and inflammation *in vivo* can improve the analysis of the efficacy of antimicrobial orthopedic biomaterials.

7. CONCLUSIONS

The identification and design of an appropriate and clinically relevant *in vivo* orthopedic implant-associated infection model to evaluate the efficacy of antimicrobial materials is dependent upon several factors including the properties of the antimicrobial material *in vivo*. For example, the degradation, antimicrobial activity, and drug release kinetics of antimicrobial materials can influence the duration of the *in vivo* study and can first be evaluated in subcutaneous pouch implantation animal models.[37,41,59,83,87,135,144,148,161]

Furthermore, the bacterial inoculum is a key design feature of the model as it is specific to the animal species of interest, the virulence of the bacterial strain, and whether the model is of acute or chronic implant-associated infection.[31,34,163–167] It is also critical to distinguish whether the antimicrobial material is intended to be used to either prevent or treat implant-associated infections as the structures of these models differ substantially (*i.e.*, models to prevent infection involve placing antimicrobial materials at time of infection and models to treat infection involve establishment of infection and debridement prior to placing antimicrobial materials).[23–25,38,94,118]

Several recent technological advances have assisted in the development of orthopedic implant-associated infection *in vivo* models that more effectively recapitulate the clinical presentation and monitor infections. These technologies include 3D-printing, bacterial genomic sequencing and microbiome profiling, and real-time *in vivo* imaging modalities.[33–37,134] These technologies have enabled the development of species-specific reproducible implants,[34,134] incorporation of patient risk factors for implant infection into the model (*e.g.*, diabetes, gut microbiome constituents),[32,33] and real-time minimally invasive tracking of infection and inflammation *in vivo*.[37] Furthermore, the emergence of stimuli-responsive antimicrobial materials (*e.g.*, responsive to temperature, magnetic/electric fields, microwaves, *etc.*) has resulted in the development of materials that can be applied minimally invasively for controlled gelling,[23,24] enable controlled release of antibiotics,[26] and enable noninvasive induction of antimicrobial activity after implantation.[27] Moving forward, emphasis can be placed on expanding imaging technologies of pathogens and antimicrobial agents (*e.g.*, tracers and tags) in preclinical models to further improve the evaluation of the efficacy of novel antimicrobial biomaterials in clinically relevant implant-associated infection models.

ACKNOWLEDGMENTS

The authors gratefully acknowledge support through National Science Foundation (NSF) Graduate Research Fellowship Program Grant No. CON501692 (E.L.C.) and support of Undergraduate Research & Creative Endeavors (SOURCE) (N.Z.), NIH NIAMS Ruth L. Kirschstein NRSA T32 AR007505 Training Program in Musculoskeletal Research (G.D.L.), NIH R01AG067997 (C.J.H.), NIH R21AR071534-01 (C.J.H.), and NIH R01GM121477 (H.A.v.R.). Additionally, the authors would like to thank Dylan Marques for assistance with the preparation of the bone wafers. Figure 1, and the Table of Contents figure were created with BioRender.com[267] (created by authors, BioRender licensing agreement/rights D34BYU0W and EM234BYOFG).

REFERENCES

(1). Wagner ER; Farley KX; Higgins I; Wilson JM; Daly CA; Gottschalk MB The incidence of shoulder arthroplasty: rise and future projections compared with hip and knee arthroplasty. J. Shoulder Elb. Surg 2020, 29, 2601–2609.

(2). Poff CB; Kothandaraman V; Kunkle BF; Friedman RJ; Eichinger JK Trends in total elbow arthroplasty utilization in the United States from 2002 to 2017. Semin. Arthroplasty JSES 2021, 31, 389.

(3). Tande AJ; Patel R Prosthetic joint infection. Clin. Microbiol. Rev 2014, 27, 302–345. [PubMed: 24696437]

(4). Triantafyllopoulos GK; Memtsoudis SG; Zhang W; Ma Y; Sculco TP; Poultsides LA Periprosthetic infection recurrence after 2-stage exchange arthroplasty: Failure or fate? J. Arthroplasty 2017, 32, 526–531. [PubMed: 27646832]

(5). Zmistowski BM; Manrique J; Patel R; Chen AF Recurrent periprosthetic joint infection after irrigation and debridement with component retention is most often due to identical organisms. J. Arthoplasty 2016, 31, 148–151.

(6). Bongers J; Jacobs AME; Smulders K; van GG; Goosen JHM Reinfection and re-revision rates of 113 two-stage revisions in infected TKA. J. Bone Jt. Infect 2020, 5, 137–144. [PubMed: 32566453]

(7). Rossmann M; Minde T; Citak M; Gehrke T; Sandiford NA; Klatte TO; Abdelaziz H High rate of reinfection with new bacteria following one-stage exchange for enterococcal periprosthetic infection of the knee: a single-center study. J. Arthroplasty 2021, 36, 711–716. [PubMed: 32863076]

(8). Schwartz AM; Farley KX; Guild GN; Bradbury TL Projections and epidemiology of revision hip and knee arthroplasty in the United States to 2030. J. Arthroplasty 2020, 35, S79–S85. [PubMed: 32151524]

(9). Adeyemi A; Trueman P Economic burden of surgical site infections within the episode of care following joint replacement. J. Orthop. Surg. Res 2019, 14, 196. [PubMed: 31248432]

(10). Tuon FF; Cieslinski J; Ono AFM; Goto FL; Machinski JM; Mantovani LK; Kosop LR; Namba MS; Rocha JL Microbiological profile and susceptibility pattern of surgical site infections related to orthopaedic trauma. Int. Orthop 2019, 43, 1309–1313. [PubMed: 30069593]

(11). Uckay I; Hoffmeyer P; Lew D; Pittet D Prevention of surgical site infections in orthopaedic surgery and bone trauma: state-of-the-art update. J. Hosp. Infect 2013, 84, 5–12. [PubMed: 23414705]

(12). Shiels SM; Bedigrew KM; Wenke JC Development of a hematogenous implant-related infection in a rat model. BMC Musculoskeletal Disord 2015, 16, 255.

(13). Wang Y; Cheng LI; Helfer DR; Ashbaugh AG; Miller RJ; Tzomides AJ; Thompson JM; Ortines RV; Tsai AS; Liu H; Dillen CA; Archer NK; Cohen TS; Tkaczyk C; Stover CK; Sellman BR; Miller LS Mouse model of hematogenous implant-related *Staphylococcus aureus* biofilm infection reveals therapeutic targets. Proc. Natl. Acad. Sci. U. S. A 2017, 114, E5094–E5102. [PubMed: 28607050]

(14). Triantafyllopoulos GK; Soranoglou V; Memtsoudis SG; Poultsides LA Implant retention after acute and hematogenous periprosthetic hip and knee infections: Whom, when and how? World J. Orthop 2016, 7, 546–552. [PubMed: 27672567]

(15). Tartari E; Weterings V; Gastmeier P; Bano JR; Widmer A; Kluytmans J; Voss A Patient engagement with surgical site infection prevention: an expert panel perspective. Antimicrob. Resist. Infect. Control 2017, 6, 45. [PubMed: 28507731]

(16). Kapadia BH; Berg RA; Daley JA; Fritz J; Bhave A; Mont MA Periprosthetic joint infection. Lancet 2016, 387, 386–394. [PubMed: 26135702]

(17). Blanco JF; Diaz A; Melchor FR; da Casa C; Pescador D Risk factors for periprosthetic joint infection after total knee arthroplasty. Arch. Orthop. Trauma Surg 2020, 140, 239–245. [PubMed: 31707484]

(18). Arciola CR; Campoccia D; Ehrlich GD; Montanaro L Biofilm-based implant infections in orthopaedics. Adv. Exp. Med. Biol 2015, 830, 29–46. [PubMed: 25366219]

(19). Wouthuyzen-Bakker M; Kheir MM; Moya I; Rondon AJ; Kheir M; Lozano L; Parvizi J; Soriano A Failure after 2-stage exchange arthroplasty for treatment of periprosthetic joint infection: the role of antibiotics in the cement spacer. Clin. Infect. Dis 2019, 68, 2087–2093. [PubMed: 30281077]

(20). van Vugt T; Arts J; Geurts J Antibiotic-loaded polymethylmethacrylate beads and spacers in treatment of orthopedic infections and the role of biofilm formation. Front. Microbiol 2019, 10, 1–11. [PubMed: 30728808]

(21). Martinez-Moreno J; Mura C; Merino V; Nacher A; Climente M; Merino-Sanjuan M Study of the influence of bone cement type and mixing method on the bioactivity and the elution kinetics of ciprofloxacin. J. Arthroplasty 2015, 30, 1243–1249. [PubMed: 25743107]

(22). Meeker DG; Cooper KB; Renard RL; Mears SC; Smeltzer MS; Barnes CL Comparative study of antibiotic elution profiles from alternative formulations of polymethylmethacrylate bone cement. J. Arthroplasty 2019, 34, 1458–1461. [PubMed: 30935799]

(23). Ter Boo G-JA; Arens D; Metsemakers W-J; Zeiter S; Richards RG; Grijpma DW; Eglin D; Moriarty TF Injectable gentamicin-loaded thermo-responsive hyaluronic acid derivative prevents infection in a rabbit model. Acta Biomater 2016, 43, 185–194. [PubMed: 27435965]

(24). Tao J; Zhang Y; Shen A; Yang Y; Diao L; Wang L; Cai D; Hu Y Injectable chitosan-based thermosensitive hydrogel/nanoparticle-loaded system for local delivery of vancomycin in the treatment of osteomyelitis. Int. J. Nanomed 2020, 15, 5855–5871.

(25). Ak G; Bozkaya UF; Yilmaz H; Turgut OS; Bilgin I; Tomruk C; Uyanikgil Y; Sanlier SH An intravenous application of magnetic nanoparticles for osteomyelitis treatment: an efficient alternative. Int. J. Pharm 2021, 592, 119999. [PubMed: 33190790]

(26). Qiao Y; Liu X; Li B; Han Y; Zheng Y; Yeung KWK; Li C; Cui Z; Liang Y; Li Z; Zhu S; Wang X; Wu S Treatment of MRSA-infected osteomyelitis using bacterial capturing, magnetically targeted composites with microwave-assisted bacterial killing. Nat. Commun 2020, 11, 4446. [PubMed: 32895387]

(27). Nodzo S; Tobias M; Hansen L; Luke-Marshall NR; Cole R; Wild L; Campagnari AA; Ehrensberger MT Cathodic electrical stimulation combined with vancomycin enhances treatment of methicillin-resistant *Staphylococcus aureus* implant-associated infections. Clin. Orthop. Relat. Res 2015, 473, 2856–2864. [PubMed: 25825157]

(28). Hui T; Yongqing X; Tiane Z; Gang L; Yonggang Y; Muyao J; Jun L; Jing D Treatment of osteomyelitis by liposomal gentamicin-impregnated calcium sulfate. Arch. Orthop. Trauma Surg 2009, 129, 1301–1308. [PubMed: 19034468]

(29). Cyphert EL; Learn GD; Hurley SK; Lu C.-y.; von Recum HA An additive to PMMA bone cement enables postimplantation drug refilling, broadens range of compatible antibiotics, and prolongs antimicrobial therapy. Adv. Healthcare Mater 2018, 7, 1800812.

(30). Ding H; Zhao C-J; Cui X; Gu Y-F; Jia W-T; Rahaman MN; Wang Y; Huang W-H; Zhang C-Q A novel injectable borate bioactive glass cement as an antibiotic delivery vehicle for treating osteomyelitis. PLoS One 2014, 9, e85472. [PubMed: 24427311]

(31). Moriarty T; Grainger D; Richards R Challenges in linking preclinical anti-microbial research strategies with clinical outcomes for device-associated infections. Euro. Cells Mater 2014, 28, 112–128.

(32). Lovati AB; Drago L; Monti L; De Vecchi E; Previdi S; Banfi G; Romano CL Diabetic mouse model of orthopaedic implant-related Staphylococcus aureus infection. PLoS One 2013, 8, e67628. [PubMed: 23818985]

(33). Hernandez CJ; Yang X; Ji G; Niu Y; Sethuraman AS; Koressel J; Shirley M; Fields MW; Chyou S; Li TM; Luna M; Callahan RL; Ross FP; Lu TT; Brito IL; Carli AV; Bostrom MPG Disruption of the gut microbiome increases the risk of periprosthetic joint infection in mice. Clin. Orthop. Relat. Res 2019, 477, 2588–2598. [PubMed: 31283731]

(34). Lopez-Torres I; Sanz-Ruiz P; Navarro-Garcia F; Leon-Roman V; Vaquero-Martin J Experimental reproduction of periprosthetic joint infection: developing a representative animal model. Knee 2020, 27, 1106–1112. [PubMed: 31982249]

(35). Ueng SW; Lin S-S; Wang I-C; Yang C-Y; Cheng R-C; Liu S-J; Chan E-C; Lai C-F; Yuan L-J; Chan S-C Efficacy of vancomycin-releasing biodegradable poly(lactic-co-glycolide) antibiotics beads for treatment of experimental bone infection due to Staphylococcus aureus. J. Orthop. Surg. Res 2016, 11, 52. [PubMed: 27121956]

(36). Lankinen P; Noponen T; Autio A; Luoto P; Frantzen J; Loyttyniemi E; Hakanen AJ; Aro HT; Roivainen A A comparative ^{68}Ga-citrate and ^{68}Ga-chloride PET/CT imaging of *Staphylococcus aureus* osteomyelitis in the rat tibia. Contrast Media Mol. Imaging 2018, 2018, 9892604. [PubMed: 29681785]

(37). Suri S; Lehman SM; Selvam S; Reddie K; Maity S; Murthy N; Garcia AJ In vivo fluorescence imaging of biomaterial-associated inflammation and infection in a minimally-invasive manner. J. Biomed. Mater. Res., Part A 2015, 103, 76–83.

(38). Ishikawa M; de Mesy Bentley KL; McEntire BJ; Bal BS; Schwarz EM; Xie C Surface topography of silicon nitride affects antimicrobial and osseointegrative properties of tibial implants in a murine model. J. Biomed. Mater. Res., Part A 2017, 105, 3413–3421.

(39). Svensson S; Suska F; Emanuelsson L; Palmquist A; Norlindh B; Trobos M; Backros H; Persson L; Rydja G; Ohrlander M; Lyven B; Lausmaa J; Thomsen P Osseointegration of titanium with an antimicrobial nanostructured noble metal coating. Nanomedicine 2013, 9, 1048–1056. [PubMed: 23639678]

(40). Aguilera-Correa J-J; Aunon A; Boiza-Sanchez M; Mahillo-Fernandez I; Mediero A; Eguibar-Blazquez D; Conde A; Arenas M-A; de-Damborenea J-J; Cordero-Ampuero J; Esteban J Urine aluminum concentration as a possible implant biomarker of *Pseudomonas aeruginosa* infection using a fluorine- and phosphorus-doped Ti-6Al-4V alloy with osseointegration capacity. ACS Omega 2019, 4, 11815–11823. [PubMed: 31460290]

(41). Xu B; Wei Q; Mettetal MR; Han J; Rau L; Tie J; May RM; Pathe ET; Reddy ST; Sullivan L; Parker AE; Maul DH; Brennan AB; Mann EE Surface micropattern reduces colonization and medical device-associated infections. J. Med. Microbiol 2017, 66, 1692–1698. [PubMed: 28984233]

(42). Li F; Li J; Huang T; Kou H; Zhou L Compression fatigue behavior and failure mechanism of porous titanium for biomedical applications. J. Mech. Behav. Biomed. Mater 2017, 65, 814–823. [PubMed: 27788474]

(43). Apostu D; Lucaciu O; Berce C; Lucaciu D; Cosma D Current methods of preventing aseptic loosening and improving osseointegration of titanium implants in cementless total hip arthroplasty: a review. J. Int. Med. Res 2018, 46, 2104–2119. [PubMed: 29098919]

(44). Abdel-Hady Gepreel M; Niinomi M Biocompatibility of Ti-alloys for long-term implantation. J. Mech. Behav. Biomed. Mater 2013, 20, 407–415. [PubMed: 23507261]

(45). Duan J; Yang Y; Zhang E; Wang H Co-Cr-Mo-Cu alloys for clinical implants with osteogenic effect by increasing bone induction, formation and development in a rabbit model. Burns Trauma 2020, 8, tkaa036.

(46). Marcomini J; Baptista C; Pascon J; Teixeira R; Reis F Investigation of a fatigue failure in a stainless steel femoral plate. J. Mech. Behav. Biomed. Mater 2014, 38, 52–58. [PubMed: 25023519]

(47). Gervais B; Vadean A; Raison M; Brochu M Failure analysis of a 316L stainless steel femoral orthopedic implant. Case Stud. Eng. Fail. Anal 2016, 5, 30–38.

(48). Manam NS; Harun WSW; Shri DNA; Ghani SAC; Kurniawan T; Ismail MH; Ibrahim MHI Study of corrosion in biocompatible metals for implants: a review. J. Alloys Compd 2017, 701, 698–715.

(49). Aboelzahab A; Azad A-M; Dolan S; Goel V Mitigation of Staphylococcus aureus-mediated surgical site infections with IR photoactivated TiO2 coatings on Ti implants. Adv. Healthcare Mater 2012, 1, 285–291.

(50). Liu L; Bhatia R; Webster TJ Atomic layer deposition of nano-TiO_2 thin films with enhanced biocompatibility and antimicrobial activity for orthopedic implants. Int. J. Nanomed 2017, 12, 8711–8723.

(51). Gasik M; Van Mellaert L; Pierron D; Braem A; Hofmans D; De Waelheyns E; Anne J; Harmand M-F; Vleugels J Reduction of biofilm infection risks and promotion of osteointegration for optimized surfaces of titanium implants. Adv. Healthcare Mater 2012, 1, 117–127.

(52). van Hengel IAJ; Tierolf MWAM; Valerio VPM; Minneboo M; Fluit AC; Fratila-Apachitei LE; Apachitei I; Zadpoor AA Self-defending additively manufactured bone implants bearing silver and copper nanoparticles. J. Mater. Chem. B 2020, 8, 1589–1602. [PubMed: 31848564]

(53). van Hengel IAJ; Putra NE; Tierolf MWAM; Minneboo M; Fluit AC; Fratila-Apachitei LE; Apachitei I; Zadpoor AA Biofunctionalization of selective laser melted porous titanium using silver and zinc nanoparticles to prevent infections by antibiotic-resistant bacteria. Acta Biomater 2020, 107, 325–337. [PubMed: 32145392]

(54). Jung WK; Koo HC; Kim KW; Shin S; Kim SH; Park YH Antibacterial activity and mechanism of action of the silver ion in Staphylococcus aureus and Escherichia coli. Appl. Environ. Microbiol 2008, 74, 2171–2178. [PubMed: 18245232]

(55). Vincent M; Duval R; Hartemann P; Engels-Deutsch M Contact killing and antimicrobial properties of copper. J. Appl. Microbiol 2018, 124, 1032–1046. [PubMed: 29280540]

(56). Norambuena GA; Patel R; Karau M; Wyles CC; Jannetto PJ; Bennet KE; Hanssen AD; Sierra RJ Antibacterial and biocompatible titanium-copper oxide coating may be a potential strategy to reduce periprosthetic infection: an in vitro study. Clin. Orthop. Relat. Res 2017, 475, 722–732. [PubMed: 26847453]

(57). Pasquet J; Chevalier Y; Pelletier J; Couval E; Bouvier D; Bolzinger M-A The contribution of zinc ions to the antimicrobial activity of zinc oxide. Colloids Surf., A 2014, 457, 263–274.

(58). Lin J; Nguyen N-YT; Zhang C; Ha A; Liu HH Antimicrobial properties of MgO nanostructures on magnesium substrates. ACS Omega 2020, 5, 24613–24627. [PubMed: 33015479]

(59). Rahim MI; Babbar A; Lienenklaus S; Pils MC; Rohde M Degradable magnesium implant-associated infections by bacterial biofilms induce robust localized and systemic inflammatory reactions in a mouse model. Biomed. Mater 2017, 12, 055006. [PubMed: 28569671]

(60). Panacek A; Kvitek L; Smekalova M; Vecerova R; Kolar M; Roderova M; Dycka F; Sebela M; Prucek R; Tomanec O; Zboril R Bacterial resistane to silver nanoparticles and how to overcome it. Nat. Nanotechnol 2018, 13, 65–71. [PubMed: 29203912]

(61). Cyphert EL; von Recum HA Emerging technologies for long-term antimicrobial device coatings: advantages and limitations. Exp. Biol. Med 2017, 242, 788–798.

(62). Cheng H; Li Y; Huo K; Gao B; Xiong W Long-lasting in vivo and in vitro antibacterial ability of nanostructured titania coating incorporated with silver nanoparticles. J. Biomed. Mater. Res., Part A 2014, 102, 3488–3499.

(63). Dakal TC; Kumar A; Majumdar RS; Yadav V Mechanistic basis of antimicrobial actions of silver nanoparticles. Front. Microbiol 2016, 7, 1831. [PubMed: 27899918]

(64). Dong Y; Zhu H; Shen Y; Zhang W; Zhang L Antibacterial activity of silver nanoparticles of different particle size against Vibrio Natriegens. PLoS One 2019, 14, e0222322. [PubMed: 31518380]

(65). Bharti S; Mukherji S; Mukherji S Enhanced antibacterial activity of decahedral silver nanoparticles. J. Nanopart. Res 2021, 23, 36.

(66). Yan X; He B; Liu L; Qu G; Shi J; Hu L; Jiang G Antibacterial mechanism of silver nanoparticles in Pseudomonas aeruginosa: proteomics approach. Metallomics 2018, 10, 557–564. [PubMed: 29637212]

(67). Chudobova D; Cihalova K; Kopel P; Melichar L; Ruttkay-Nedecky B; Vaculovicova M; Adam V; Kizek R Complexes of metal-based nanoparticles with chitosan suppressing the risk of *Staphylococcus aureus* and *Escherichia coli* infections. In Nanotechnology in Diagnosis, Treatment and Prophylaxis of Infectious Diseases; Rai M, Kon K, Eds.; Academic Press, 2015, Chapter 13, pp 217–232.

(68). Hattori K; Nakadate K; Morii A; Noguchi T; Ogasawara Y; Ishii K Exposure to nano-size titanium dioxide causes oxidative damages in human mesothelial cells: the crystal form rather than size of particle contributed to cytotoxicity. Biochem. Biophys. Res. Commun 2017, 492, 218–223. [PubMed: 28823918]

(69). Lecka K; Gasiorek J; Mazur-Nowacka A; Szczygiel B; Antonczak A Adhesion and corrosion resistance of laser-oxidized titanium in potential biomedical application. Surf. Coat. Technol 2019, 366, 179–189.

(70). Azizi-Lalabadi M; Ehsani A; Divband B; Alizadeh-Sani M Antimicrobial activity of titanium dioxide and zinc oxide nanoparticles supported in 4A zeolite and evaluation the morphological characteristic. Sci. Rep 2019, 9, 17439. [PubMed: 31767932]

(71). Smith A; Kelton R; Meletis EI Deposition of Ni Coatings by Electrolytic Plasma Processing. Plasma Chem. Plasma Process 2015, 35, 963–978.

(72). Sansone V; Pagani D; Melato M The effects on bone cells of metal ions released from orthopaedic implants. A review. Clin. Cases Min. Bone Metab 2013, 10, 34–40.

(73). Li Y; Wong C; Xiong J; Hodgson P; Wen C Cytotoxicity of titanium and titanium alloying elements. J. Dent. Res 2010, 89, 493–497. [PubMed: 20332331]

(74). Kanaji A; Orhue V; Caicedo MS; Virdi AS; Sumner DR; Hallab NJ; Yoshiaki T; Sena K Cytotoxic effects of cobalt and nickel ions on osteocytes in vitro. J. Orthop. Surg. Res 2014, 9, 91. [PubMed: 25288055]

(75). Zhu W-Q; Ming P-P; Qiu J; Shao S-Y; Yu Y-J; Chen JX; Yang J; Xu L-N; Zhang S-M; Tang C-B Effect of titanium ions on the Hippo/YAP signaling pathway in regulating biological behaviors of MC3T3-E1 osteoblasts. J. Appl. Toxicol 2018, 38, 824–833. [PubMed: 29377205]

(76). Semisch A; Ohle J; Witt B; Hartwig A Cytotoxicity and genotoxicity of nano- and microparticulate copper oxide: role of solubility and intracellular bioactivity. Part. Fibre Toxicol 2014, 11, 10. [PubMed: 24520990]

(77). Beer C; Foldbjerg R; Hayashi Y; Sutherland DS; Autrup H Toxicity of silver nanoparticles – nanoparticle or silver ion? Toxicol. Lett 2012, 208, 286–292. [PubMed: 22101214]

(78). Liao M; Liu H Gene expression profiling of nephrotoxicity from copper nanoparticles in rats after repeated oral administration. Environ. Toxicol. Pharmacol 2012, 34, 67–80. [PubMed: 22465980]

(79). Liu Y; Sun L; Yang G; Yang Z Nephrotoxicity and genotoxicity of silver nanoparticles in juvenile rats and possible mechanism of action. Arh. Hig. Rada Toksikol 2020, 71, 121–129. [PubMed: 32975098]

(80). Zhu Y; Costa M Metals and molecular carcinogenesis. Carcinogenesis 2020, 41, 1161–1172. [PubMed: 32674145]

(81). Costerton J; Stewart P; Greenberg E Bacterial biofilms: a common cause of persistent infections. Science 1999, 284, 1318–1322. [PubMed: 10334980]

(82). Zhang X; Brodus D; Hollimon V; Hu H A brief review of recent development in the designs that prevent bio-fouling on silicon and silicon-based materials. Chem. Cent. J 2017, 11, 18. [PubMed: 28261323]

(83). Pawar V; Bulbake U; Khan W; Srivastava R Chitosan sponges as a sustained release carrier system for the prophylaxis of orthopedic implant-associated infections. Int. J. Biol. Macromol 2019, 134, 100–112. [PubMed: 31055114]

(84). Romano C; Vecchi ED; Bortolin M; Morelli I; Drago L Hyaluronic acid and its composites as a local antimicrobial/antiadhesive barrier. J. Bone Jt. Infect 2017, 2, 63–72. [PubMed: 28529865]

(85). Jung SW; Oh SH; Lee IS; Byun J-H; Lee JH In situ gelling hydrogel with anti-bacterial activity and bone healing property for treatment of osteomyelitis. Tissue Eng. Regener. Med 2019, 16, 479–490.

(86). Mendel V; Simanowski H-J; Scholz H; Heymann H Therapy with gentamicin-PMMA beads, gentamicin-collagen sponge, and cefazolin for experimental osteomyelitis due to Staphylococcus aureus in rats. Arch. Orthop. Trauma Surg 2005, 125, 363–368. [PubMed: 15864679]

(87). Hart E; Azzopardi K; Taking H; Graichen F; Jeffery J; Mayadunne R; Wickramaratna M; O'Shea M; Nijagal B; Watkinson R; O'Leary S; Finnin B; Tait R; Robins-Browne R Efficacy of antimicrobial polymer coatings in an animal model of bacterial infection associated with foreign body implants. J. Antimicrob. Chemother 2010, 65, 974–980. [PubMed: 20233779]

(88). Argarate N; Olalde B; Atorrasagasti G; Valero J; Cifuentes SC; Benavente R; Lieblich M; Gonzalez-Carrasco J Biodegradable Bi-layered coating on polymeric orthopaedic implants for controlled release of drugs. Mater. Lett 2014, 132, 193–195.

(89). Kaur S; Harjai K; Chhibber S Local delivery of linezolid from poly-d,l-lactide (PDLLA)-linezolid-coated orthopaedic implants to prevent MRSA mediated post-arthroplasty infections. Diagn. Microbiol. Infect. Dis 2014, 79, 387–392. [PubMed: 24809862]

(90). Hegde V; Park HY; Dworsky E; Zoller SD; Xi W; Johansen DO; Loftin AH; Hamad CD; Segura T; Bernthal NM The use of a novel antimicrobial implant coating in vivo to prevent spinal implant infection. Spine 2020, 45, E305–E311. [PubMed: 31593059]

(91). Stavrakis AI; Zhu S; Hegde V; Loftin AH; Ashbaugh AG; Niska JA; Miller LS; Segura T; Bernthal NM In vivo efficacy of a "smart" antimicrobial implant coating. J. Bone Joint Surg. Am 2016, 98, 1183–1189. [PubMed: 27440566]

(92). Stavrakis AI; Zhu S; Loftin AH; Weixian X; Niska J; Hegde V; Segura T; Bernthal NM Controlled release of vancomycin and tigecycline from an orthopaedic implant coating prevents Staphylococcus aureus infection in an open fracture animal model. BioMed Res. Int 2019, 2019, 1638508. [PubMed: 31915682]

(93). Bernthal NM; Stavrakis AI; Billi F; Cho JS; Kremen TJ; Simon SI; Cheung AL; Finerman GA; Lieberman JR; Adams JS; Miller LS A mouse model of post-arthroplasty Staphylococcus aureus

joint infection to evaluate in vivo the efficacy of antimicrobial implant coatings. PLoS One 2010, 5, e12580. [PubMed: 20830204]

(94). Lucke M; Schmidmaier G; Sadoni S; Wildemann B; Schiller R; Haas NP; Raschke M Gentamicin coating of metallic implants reduces implant-related osteomyelitis in rats. Bone 2003, 32, 521–531. [PubMed: 12753868]

(95). Lucke M; Wildemann B; Sadoni S; Surke C; Schiller R; Stemberger A; Rascheke M; Haas NP; Schmidmaier G Systemic versus local application of gentamicin in prophylaxis of implant-related osteomyelitis in a rat model. Bone 2005, 36, 770–778. [PubMed: 15794930]

(96). Vester H; Wildemann B; Schmidmaier G; Stockle U; Lucke M Gentamycin delivered from a PDLLA coating of metallic implants in vivo and in vitro characterization for local prophylaxis of implant-related osteomyelitis. Injury 2010, 41, 1053–1059. [PubMed: 20541756]

(97). Min J; Choi KY; Dreaden EC; Padera RF; Braatz RD; Spector M; Hammond PT Designer dual therapy nanolayered implant coatings eradicate biofilms and accelerate bone tissue repair. ACS Nano 2016, 10, 4441–4450. [PubMed: 26923427]

(98). Hasan R; Schaner K; Schroeder M; Wohlers A; Shreffler J; Schaper C; Subramanian H; Brooks A Extended release combination antibiotic therapy from a bone void filling putty for treatment of osteomyelitis. Pharmaceutics 2019, 11, 592. [PubMed: 31717467]

(99). Croes M; Bakhshandeh S; van Hengel IAJ; Lietaert K; van Kessel KPM; Pouran B; van der Wal BCH; Vogely HC; Van Hecke W; Fluit AC; Boel CHE; Alblas J; Zadpoor AA; Weinans H; Yavari SA Antibacterial and immunogenic behavior of silver coatings on additively manufactured porous titanium. Acta Biomater 2018, 81, 315–327. [PubMed: 30268917]

(100). Miller RJ; Thompson JM; Zheng J; Marchitto MC; Archer NK; Pinsker BL; Ortines RV; Jiang X; Martin RA; Brown ID; Wang Y; Sterling RS; Mao H-Q; Miller LS In vivo bioluminescence imaging in a rabbit model of orthopaedic implant-associated infection to monitor efficacy of an antibiotic-releasing coating. J. Bone Joint Surg. Am 2019, 101, e12. [PubMed: 30801375]

(101). Ambrose CG; Clyburn TA; Mika J; Gogola GR; Kaplan HB; Wanger A; Mikos AG Evaluation of antibiotic-impregnated microspheres for the prevention of implant-associated orthopaedic infections. J. Bone Joint Surg. Am 2014, 96, 128–134. [PubMed: 24430412]

(102). Giavaresi G; Meani E; Sartori M; Ferrari A; Bellini D; Sacchetta AC; Meraner J; Sambri A; Vocale C; Sambri V; Fini M; Romano CL Efficacy of antibacterial-loaded coating in an in vivo model of acutely highly contaminated implant. Int. Orthop 2014, 38, 1505–1512. [PubMed: 24363076]

(103). Ferrell Z; Grainger D; Sinclair K Antibiotic-eluting resorbable bone-void filler evaluated in a large animal infection prevention model. Eur. Cell Mater 2019, 37, 265–276. [PubMed: 30957870]

(104). McLaren JS; White LJ; Cox HC; Ashraf W; Rahman CV; Blunn GW; Goodship AE; Quirk RA; Shakesheff KM; Bayston R; Scammell BE A biodegradable antibiotic-impregnated scaffold to prevent osteomyelitis in a contaminated in vivo bone defect model. Euro. Cells Mater 2014, 27, 332–349.

(105). Cobb LH; Park J; Swanson EA; Beard MC; McCabe EM; Rourke AS; Seo KS; Olivier AK; Priddy LB CRISPRCas9 modified bacteriophage for treatment of Staphylococcus aureus induced osteomyelitis and soft tissue infection. PLoS One 2019, 14, e0220421. [PubMed: 31756187]

(106). Yan L; Jiang D-M; Cao Z-D; Wu J; Wang X; Wang ZL; Li Y-J; Yi Y-F Treatment of Staphylococcus aureus-induced chronic osteomyelitis with bone-like hydroxyapatite/poly amino acid loaded with rifapentine microspheres. Drug Des., Dev. Ther 2015, 9, 3665–3676.

(107). Felfel RM; Ahmed I; Parsons AJ; Haque P; Walker GS; Rudd CD Investigation of crystallinity, molecular weight change, and mechanical properties of PLA/PBG bioresorbable composites as bone fracture fixation plates. J. Biomater. Appl 2012, 26, 765–789. [PubMed: 21123285]

(108). Yuan Y; Chesnutt BM; Haggard WO; Bumgardner JD Deacetylation of chitosan: material characterization and in vitro evaluation via albumin adsorption and pre-osteoblastic cell cultures. Materials 2011, 4, 1399–1416. [PubMed: 28824150]

(109). Hahn SK; Park JK; Tomimatsu T; Shimoboji T Synthesis and degradation test of hyaluronic acid hydrogels. Int. J. Biol. Macromol 2007, 40, 374–380. [PubMed: 17101173]

(110). Makadia HK; Siegel SJ Poly lactic-co-glycolic acid (PLGA) as biodegradable controlled drug delivery carrier. Polymers 2011, 3, 1377–1397. [PubMed: 22577513]

(111). Meng X; Lu Y; Gao Y; Cheng S; Tian F; Xiao Y; Li F Chitosan/alginate/hyaluronic acid polyelectrolyte composite sponges crosslinked with genepin for wound dressing application. Int. J. Biol. Macromol 2021, 182, 512–523. [PubMed: 33848546]

(112). Yang C; Ouyang L; Wang W; Chen B; Liu W; Yuan X; Luo Y; Cheng T; Yeung KWK; Liu X; Zhang X Sodium butyrate-modified sulfonated polyetheretherketone modulates macrophage behavior and shows enhanced antibacterial and osteogenic functions during implant-associated infections. J. Mater. Chem. B 2019, 7, 5541–5553. [PubMed: 31451811]

(113). Xue Z; Wang Z; Sun A; Huang J; Wu W; Chen M; Hao X; Huang Z; Lin X; Weng S Rapid construction of polyetheretherketone (PEEK) biological implants incorporated with brushite ($CaHPO_4$ $2H_2O$) and antibiotics for anti-infection and enhanced osseointegration. Mater. Sci. Eng., C 2020, C111, 110782.

(114). Liu W; Li J; Cheng M; Wang Q; Qian Y; Yeung KWK; Chu PK; Zhang X A surface-engineered polyetheretherketone biomaterial implant with direct and immunoregulatory antibacterial activity against methicillin-resistant Staphylococcus aureus. Biomaterials 2019, 208, 8–20. [PubMed: 30986611]

(115). Rochford ETJ; Bresco MS; Poulsson AHC; Kluge K; Zeiter S; Ziegler M; O'Mahony L; Richards RG; Moriarty TF Infection burden and immunological responses are equivalent for polymeric and metallic implant materials in vitro and in a murine model of fracture-related infection. J. Biomed. Mater. Res., Part B 2019, 107, 1095–1106.

(116). Stadelmann VA; Thompson K; Zeiter S; Camenisch K; Styger U; Patrick S; McDowell A; Nehrbass D; Richards RG; Moriarty TF Longitudinal time-lapse in vivo micro-CT reveals differential patterns of peri-implant bone changes after subclinical bacterial infection in a rat model. Sci. Rep 2020, 10, 20901. [PubMed: 33262377]

(117). Stadelmann VA; Potapova I; Camenisch K; Nehrbass D; Richards RG; Moriarty TF In vivo microCT monitoring of osteomyelitis in a rat model. BioMed Res. Int 2015, 2015, 587857. [PubMed: 26064928]

(118). Inzana JA; Trombetta RP; Schwarz EM; Kates SL; Awad HA 3D printed bioceramics for dual antibiotic delivery to treat implant-associated bone infection. Eur. Cell. Mater 2015, 30, 232–247. [PubMed: 26535494]

(119). Inzana JA; Schwarz EM; Kates SL; Awad HA A novel murine model of established staphylococcal bone infection in the presence of a fracture fixation plate to study therapies utilizing antibiotic-laden spacers after revision surgery. Bone 2015, 72, 128–136. [PubMed: 25459073]

(120). Johnson CT; Wroe JA; Agarwal R; Martin KE; Guldberg RE; Donlan RM; Westblade LF; Garcia AJ Hydrogel delivery of lysostaphin eliminates orthopedic implant infection by Staphylococcus aureus and supports fracture healing. Proc. Natl. Acad. Sci. U. S. A 2018, 115, E4960–E4969. [PubMed: 29760099]

(121). Walther R; Nielsen SM; Christiansen R; Meyer RL; Zelikin AN Combatting implant-associated biofilms through localized drug synthesis. J. Controlled Release 2018, 287, 94–102.

(122). Sun Y; Zhao Y-Q; Zeng Q; Wu Y-W; Hu Y; Duan S; Tang Z; Xu F-J Dual-functional implants with antibacterial and osteointegration-promoting performances. ACS Appl. Mater. Interfaces 2019, 11, 36449–36457. [PubMed: 31532178]

(123). Cyphert EL; Lu C.-y.; Marques DW; Learn GD; von Recum HA Combination antibiotic delivery in PMMA provides sustained broad-spectrum antimicrobial activity and allows for postimplantation refilling. Biomacromolecules 2020, 21, 854–866. [PubMed: 31877029]

(124). Cyphert EL; Learn GD; Marques DW; Lu C-y.; von Recum, H. A. Antibiotic refilling, antimicrobial activity, and mechanical strength of PMMA bone cement composites critically depend on the processing technique. ACS Biomater. Sci. Eng 2020, 6, 4024–4035. [PubMed: 33463344]

(125). Cyphert EL; Zhang N; Marques DW; Learn GD; Zhang F; von Recum HA Poly(methyl methacrylate) bone cement composite can be refilled with antibiotics after implantation in femur or soft tissue. J. Funct. Biomater 2021, 12, 8. [PubMed: 33530542]

(126). Trombetta R; de Mesy Bentley K; Schwarz E; Kate S; Awad H A murine femoral ostectomy model with hardware exchange to assess antibiotic-impregnated spacers for implant-associated osteomyelitis. Eur. Cell. Mater 2019, 37, 431–443. [PubMed: 31243755]

(127). Carli AV; Bhimani S; Yang X; de Mesy Bentley KL; Ross FP; Bostrom MP Vancomycin-loaded polymethylmethacrylate spacers fail to eradicate periprosthetic joint infection in a clinically representative mouse model. J. Bone Jt. Surg 2018, 100, e76.

(128). Morris JL; Letson HL; Grant A; Wilkinson M; Hazratwala K; McEwen P Experimental model of peri-prosthetic infection of the knee caused by Staphylococcus aureus using biomaterials representative of modern TKA. Biol. Open 2019, 8, bio045203.

(129). Tuzuner T; Sencan I; Ozdemir D; Alper M; Duman S; Yavuz T; Yildirim M In vivo evaluation of teicoplanin- and calcium sulfate-loaded PMMA bone cement in preventing implant-related osteomyelitis in rats. J. Chemother 2006, 18, 628–633. [PubMed: 17267341]

(130). Wenke J; Owens B; Svoboda S; Brooks D Effectiveness of commercially-available antibiotic-impregnated implants. J. Bone Jt. Surg., Br. Vol 2006, 88B, 1102–1104.

(131). Ersoz G; Oztuna V; Coskun B; Eskandari M; Bayarslan C; Kaya A Addition of fusidic acid impregnated bone cement to systemic teicoplanin therapy in the treatment of rat osteomyelitis. J. Chemother 2004, 16, 51–55.

(132). Brunotte M; Rupp M; Stotzel S; Sommer U; Mohammed W; Thormann U; Heiss C; Lips KS; Domann E; Alt V A new small animal model for simulating a two-stage-revision procedure in implant-related methicillin-resistant Staphylococcus aureus bone infection. Injury 2019, 50, 1921–1928. [PubMed: 31451184]

(133). Mauerer A; Stenglein S; Schulz-Drost S; Schorner C; Taylor D; Krinner S; Heidenau F; Adler W; Forst R Antibacterial effect of a 4x Cu-TiO_2 coating simulating acute periprosthetic infection – an animal model. Molecules 2017, 22, 1042. [PubMed: 28644421]

(134). Lopez-Torres I; Sanz-Ruiz P; Leon-Roman V; Navarro-Garcia F; Priego-Sanchez R; Vaquero-Martin J 3D printing in experimental orthopaedic surgery: do it yourself. Eur. J. Orthop. Surg. Traumatol 2019, 29, 967–972. [PubMed: 30864016]

(135). Nablo BJ; Prichard HL; Butler RD; Klitzman B; Schoenfisch MH Inhibition of implant-associated infections via nitric oxide release. Biomaterials 2005, 26, 6984–6990. [PubMed: 15978663]

(136). Khansarizadeh M; Mokhtarzadeh A; Rashedinia M; Taghdisi SM; Lari P; Abnous KH; Ramezani M Identification of possible cytotoxicity mechanism of polyethylenimine by proteomics analysis. Hum. Exp. Toxicol 2016, 35, 377–387. [PubMed: 26134983]

(137). Kurtz SM; Devine JN PEEK biomaterials in trauma, orthopedic, and spinal implants. Biomaterials 2007, 28, 4845–4869. [PubMed: 17686513]

(138). Liu X; Cheng C; Peng X; Xiao H; Guo C; Wang X; Li L; Yu X A promising material for bone repair: PMMA bone cement modified by dopamine-coated strontium-doped calcium polyphosphate particles. R. Soc. Open Sci 2019, 6, 191028. [PubMed: 31824710]

(139). Daghighi S; Sjollema J; van der Mei HC; Busscher HJ; Rochford ET Infection resistance of degradable versus nondegradable biomaterials: an assessment of the potential mechanisms. Biomaterials 2013, 34, 8013–8017. [PubMed: 23915949]

(140). Cyphert EL; Zuckerman ST; Korley JN; von Recum HA Affinity interactions drive post-implantation drug filling, even in the presence of bacterial biofilm. Acta Biomater 2017, 57, 95–102. [PubMed: 28414173]

(141). Pforringer D; Harrasser N; Muhlhofer H; Kiokekli M; Stemberger A; van Griensven M; Lucke M; Burgkart R; Obermeier A Osteoinduction and -conduction through absorbable bone substitute materials based on calcium sulfate: in vivo biological behavior in a rabbit model. J. Mater. Sci.: Mater. Med 2018, 29, 17. [PubMed: 29318379]

(142). Pforringer D; Obermeier A; Kiokekli M; Buchner H; Vogt S; Stemberger A; Burgkart R; Lucke M Antimicrobial formulations of absorbable bone substitute materials as drug carriers based on calcium sulfate. Antimicrob. Agents Chemother 2016, 60, 3897–3905. [PubMed: 27067337]

(143). Wang Y; Wang X; Li H; Xue D; Shi Z; Qi Y; Ma Q; Pan Z Assessing the character of the rhBMP-2- and vancomycin-loaded calcium sulphate composites in vitro and in vivo. Arch. Orthop. Trauma Surg 2011, 131, 991–1001. [PubMed: 21318424]

(144). Qayoom I; Teotia AK; Panjla A; Verma S; Kumar A Local and sustained delivery of rifampicin from a bioactive ceramic carrier treats bone infection in a rat tibia. ACS Infect. Dis 2020, 6, 2938–2949. [PubMed: 32966037]

(145). Jiang N; Dusane DH; Brooks JR; Delury CP; Aiken SS; Laycock PA; Stoodley P Antibiotic loaded β-tricalcium phosphate/calcium sulfate for antimicrobial potency, prevention and killing efficacy of Pseudomonas aeruginosa and Staphylococcus aureus biofilms. Sci. Rep 2021, 11, 1446. [PubMed: 33446860]

(146). Huang Y; Song G; Chang X; Wang Z; Zhang X; Han S; Su Z; Yang H; Yang D; Zhang X Nanostructured Ag^{+}-substituted fluorhydroxyapatite-TiO_2 coatings for enhanced bactericidal effects and osteoinductivity of Ti for biomedical applications. Int. J. Nanomed 2018, 13, 2665–2684.

(147). Pan J; Prabakaran S; Rajan M In-vivo assessment of minerals substituted hydroxyapatite/poly sorbitol sebacate glutamate (PSSG) composite coating on titanium metal implant for orthopedic implantation. Biomed. Pharmacother 2019, 119, 109404. [PubMed: 31526972]

(148). Ueno M; Miyamoto H; Tsukamoto M; Eto S; Noda I; Shobuike T; Kobatake T; Sonohata M; Mawatari M Silver-containing hydroxyapatite coating reduces biofilm formation by methicillin-resistant Staphylococcus aureus in vitro and in vivo. BioMed Res. Int 2016, 2016, 8070597. [PubMed: 28105433]

(149). Pilz M; Staats K; Tobudic S; Assadian O; Presterl E; Windhager R; Holinka J Zirconium nitride coating reduced Staphylococcus epidermidis biofilm formation on orthopaedic implant surfaces: an in vitro study. Clin. Orthop. Relat. Res 2019, 477, 461–466. [PubMed: 30418277]

(150). Kose N; Otuzbir A; Peksen C; Kiremitci A; Dogan A A silver ion-doped calcium phosphate-based ceramic nanopowder-coated prosthesis increased infection resistance. Clin. Orthop. Relat. Res 2013, 471, 2532–2539. [PubMed: 23463287]

(151). Drnovsek N; Novak S; Dragin U; Ceh M; Gorensek M; Gradisar M Bioactive glass enhances bone ingrowth into the porous titanium coating on orthopaedic implants. Int. Orthop 2012, 36, 1739–1745. [PubMed: 22422142]

(152). Wu VM; Huynh E; Tang S; Uskokovic V Calcium phosphate nanoparticles as intrinsic organic antimicrobials: mechanism of action. Biomed. Mater 2021, 16, 015018.

(153). Lu J; Descamps M; Dejou J; Koubi G; Hardouin P; Lemaitre J; Proust J-P The biodegradation mechanism of calcium phosphate biomaterials in bone. J. Biomed. Mater. Res 2002, 63, 408–412. [PubMed: 12115748]

(154). Yang N; Zhong Q; Zhou Y; Kundu SC; Yao J; Cai Y Controlled degradation pattern of hydroxyapatite/calcium carbonate composite microspheres. Microsc. Res. Tech 2016, 79, 518–524. [PubMed: 27037606]

(155). Su Y; Cockerill I; Zheng Y; Tang L; Qin Y-X; Zhu D Biofunctionalization of metallic implants by calcium phosphate coatings. Bioact. Mater 2019, 4, 196–206. [PubMed: 31193406]

(156). Landis WJ; Jacquet R Association of calcium and phosphate ions with collagen in the mineralization of vertebrate tissues. Calcif. Tissue Int 2013, 93, 329–337. [PubMed: 23543143]

(157). Kose N; Caylak R; Peksen C; Kiremitci A; Burukoglu D; Koparal S; Dogan A Silver ion doped ceramic nano-powder coated nails prevent infection in open fractures: In vivo study. Injury 2016, 47, 320–324. [PubMed: 26589596]

(158). Anagnostakos K; Kelm J Enhancement of antibiotic elution from acrylic bone cement. J. Biomed. Mater. Res., Part B 2009, 90B, 467–475.

(159). Bidossi A; Bottagisio M; De Grandi R; De Vecchi E Ability of adhesion and biofilm formation of pathogens of periprosthetic joint infections on titanium-niobium nitride (TiNbN) ceramic coatings. J. Orthop. Surg. Res 2020, 15, 90. [PubMed: 32131862]

(160). Hu X; Neoh K-G; Shi Z; Kang E-T; Poh C; Wang W An in vitro assessment of titanium functionalized with polysaccharides conjugated with vascular endothelial growth factor for enhanced osseointegration and inhibition of bacterial adhesion. Biomaterials 2010, 31, 8854–8863. [PubMed: 20800276]

(161). Han J; Yang Y; Lu J; Wang C; Xie Y; Zheng X; Yao Z; Zhang C Sustained release vancomycin-coated titanium alloy using a novel electrostatic dry powder coating technique may be a potential

strategy to reduce implant-related infection. BioSci. Trends 2017, 11, 346–354. [PubMed: 28552898]

(162). Perez LM; Lalueza P; Monzon M; Puertolas JA; Arruebo M; Santamaria J Hollow porous implants filled with mesoporous silica particles as a two-stage antibiotic-eluting device. Int. J. Pharm 2011, 409, 1–8. [PubMed: 21335077]

(163). Thompson JM; Miller RJ; Ashbaugh AG; Dillen CA; Pickett JE; Wang Y; Ortines RV; Sterling RS; Francis KP; Bernthal NM; Cohen TS; Tkaczyk C; Yu L; Stover CK; DiGiandomenico A; Sellman BR; Thorek DL; Miller LS Mouse model of Gram-negative prosthetic joint infection reveals therapeutic targets. JCI Insight 2018, 3, e121737. [PubMed: 30185667]

(164). Zhai H; Pan J; Pang E; Bai B Lavage with allicin in combination with vancomycin inhibits biofilm formation by Staphylococcus epidermidis in a rabbit model of prosthetic joint infection. PLoS One 2014, 9, e102760. [PubMed: 25025650]

(165). Meulemans L; Hermans K; Duchateau L; Haesebrouck F High and low virulence Staphylococcus aureus strains in a rabbit skin infection model. Vet. Microbiol 2007, 125, 333–340. [PubMed: 17644278]

(166). Marculescu C; Berbari EF; Cockerill FR; Osmon DR Unusual aerobic and anaerobic bacteria associated with prosthetic joint infections. Clin. Orthop. Relat. Res 2006, 451, 55–63. [PubMed: 16906072]

(167). Francois EL; Yaszemski MJ Chapter 43-Preclinical bone repair models in regenerative medicine. In Principles of regenerative medicine 2019, 761–767.

(168). Jie K; Deng P; Cao H; Feng W; Chen J; Zeng Y Prosthesis design of animal models of periprosthetic joint infection following total knee arthroplasty: a systematic review. PLoS One 2019, 14, e0223402. [PubMed: 31581252]

(169). Tomecka MJ; Ethiraj LP; Sanchez LM; Roehl HH; Carney TJ Clinical pathologies of bone fracture modelled in zebrafish. Dis. Models Mech 2019, 12, dmm037630.

(170). Windolf CD; Meng W; Logters TT; MacKenzie CR; Windolf J; Flohe S Implant-associated localized osteitis in murine femur fracture by biofilm forming Staphylococcus aureus: a novel experimental model. J. Orthop. Res 2013, 31, 2013–2020. [PubMed: 23878009]

(171). Buren C; Hambuchen M; Windolf J; Logters T; Windolf CD Histological score for degrees of severity in an implant-associated infection model in mice. Arch. Orthop. Trauma Surg 2019, 139, 1235–1244. [PubMed: 31020411]

(172). Masters EA; Hao SP; Kenney HM; Morita Y; Galloway CA; de Mesy Bentley KL; Ricciardi BF; Boyce BF; Schwarz EM; Oh I Distinct vasculotropic versus osteotropic features of S. agalactiae versus S. aureus implant-associated bone infection in mice. J. Orthop. Res 2021, 39, 389–401. [PubMed: 33336806]

(173). Carli AV; Bhimani S; Yang X; Shirley MB; de Mesy Bentley KL; Ross FP; Bostrom MPG Quantification of peri-implant bacterial load and in vivo biofilm formation in an innovative, clinically representative mouse model of periprosthetic joint infection. J. Bone Joint Surg. Am 2017, 99, e25. [PubMed: 28291188]

(174). Sheppard WL; Mosich GM; Smith RA; Hamad CD; Park HY; Zoller SD; Trikha R; McCoy TK; Borthwell R; Hoang J; Truong N; Cevallos N; Clarkson S; Hori KR; van Dijl JM; Francis KP; Petrigliano FA; Bernthal NM Novel in vivo mouse model of shoulder implant infection. J. Shoulder Elbow Surg 2020, 29, 1412–1424. [PubMed: 32014357]

(175). Nishitani K; Sutipornpalangkul W; de Mesy Bentley KL; Varrone JJ; Bello-Irizarry SN; Ito H; Matsuda S; Kates SL; Daiss JL; Schwarz EM Quantifying the natural history of biofilm formation in vivo during the establishment of chronic implant-associated Staphylococcus aureus osteomyelitis in mice to identify critical pathogen and host factors. J. Orthop. Res 2015, 33, 1311–1319. [PubMed: 25820925]

(176). Haenle M; Zietz C; Lindner T; Arndt K; Vetter A; Mittelmeier W; Podbielski A; Bader R A model of implant-associated infection in the tibial metaphysis of rats. Sci. World J 2013, 2013, 481975.

(177). Lucke M; Schmidmaier G; Sadoni S; Wildemann B; Schiller R; Stemberger A; Haas NP; Raschke M A new model of implant-related osteomyelitis in rats. J. Biomed. Mater. Res 2003, 67B, 593–602.

(178). Søe NH; Jensen NV; Nurnberg BM; Jensen AL; Koch J; Poulsen SS; Pier G; Johansen HK A novel knee prosthesis model of implant-related osteomyelitis in rats. Acta Orthop 2013, 84, 92–97. [PubMed: 23409845]

(179). Fan Y; Xiao Y; Sabuhi WA; Leape CP; Gil D; Grindy S; Muratoglu OK; Bedair H; Collins JE; Randolph M; Oral E Longitudinal model of periprosthetic joint infection in the rat. J. Orthop. Res 2020, 38, 1101–1112. [PubMed: 31808572]

(180). Zhu H; Bao B; Wei H; Gao T; Chai Y; Zhang C; Zheng X Is EDTA irrigation effective in reducing bacterial infection in a rat model of contaminated intra-articular knee implants? Clin. Orthop. Relat. Res 2020, 478, 1111–1121. [PubMed: 32012144]

(181). Zhang X; Ma Y-F; Wang L; Jiang N; Qin C-H; Hu Y-J; Yu B A rabbit model of implant-related osteomyelitis inoculated with biofilm after open femoral fracture. Exp. Ther. Med 2017, 14, 4995–5001. [PubMed: 29201204]

(182). Odekerken JC; Arts JJ; Surtel DA; Walenkamp GH; Welting TJ A rabbit osteomyelitis model for the longitudinal assessment of early post-operative implant infections. J. Orthop. Surg. Res 2013, 8, 38. [PubMed: 24188807]

(183). Gahukamble AD; McDowell A; Post V; Varela JS; Rochford ETJ; Richards RG; Patrick S; Moriarty TF Propionibacterium acnes and Staphylococcus lugdunensis cause pyogenic osteomyelitis in an intramedullary nail model in rabbits. J. Clin. Microbiol 2014, 52, 1595–1606. [PubMed: 24599975]

(184). Jensen LK; Koch J; Dich-Jorgensen K; Aalbaek B; Petersen A; Fuursted K; Bjarnsholt T; Kragh KN; Totterup M; Bue M; Hanberg P; Soballe K; Heegaard PMH; Jensen HE Novel porcine model of implant-associated osteomyelitis: a comprehensive analysis of local, regional, and systemic response. J. Orthop. Res 2017, 35, 2211–2221. [PubMed: 27958656]

(185). Johansen LK; Koch J; Frees D; Aalbaek B; Nielsen OL; Leifsson PS; Iburg TM; Svalastoga E; Buelund LE; Bjarnsholt T; Hoiby N; Jensen HE Pathology and biofilm formation in a porcine model of staphylococcal osteomyelitis. J. Comp. Pathol 2012, 147, 343–353. [PubMed: 22534025]

(186). Funao H; Nagai S; Sasaki A; Hoshikawa T; Tsuji T; Okada Y; Koyasu S; Toyama Y; Nakamura M; Aizawa M; Matsumoto M; Ishii K A novel hydroxyapatite film coated with ionic silver via inositol hexaphosphate chelation prevents implant-associated infection. Sci. Rep 2016, 6, 23238. [PubMed: 26984477]

(187). Ishihama H; Ishii K; Nagai S; Kakinuma H; Sasaki A; Yoshioka K; Kuramoto T; Shiono Y; Funao H; Isogai N; Tsuji T; Okada Y; Koyasu S; Toyama Y; Nakamura M; Aizawa M; Matsumoto M An antibacterial coated polymer prevents biofilm formation and implant-associated infection. Sci. Rep 2021, 11, 3602. [PubMed: 33574464]

(188). Niska JA; Shahbazian JH; Ramos RI; Pribaz JR; Billi F; Francis KP; Miller LS Daptomycin and tigecycline have broader effective dose ranges than vancomycin as prophylaxis against a Staphylococcus aureus surgical implant infection in mice. Antimicrob. Agents Chemother 2012, 56, 2590–2597. [PubMed: 22371896]

(189). Lovati AB; Bottagisio M; Maraldi S; Violatto MB; Bortolin M; De Vecchi E; Bigini P; Drago L; Romano CL Vitamin E phosphate coating stimulates bone deposition in implant-related infections in a rat model. Clin. Orthop. Relat. Res 2018, 476, 1324–1338. [PubMed: 29771856]

(190). Lulu GA; Karunanidhi A; Yusof LM; Abba Y; Fauzi FM; Othman F In vivo efficacy of tobramycin-loaded synthetic calcium phosphate beads in a rabbit model of staphylococcal osteomyelitis. Ann. Clin. Microbiol. Antimicrob 2018, 17, 46. [PubMed: 30593272]

(191). Koh I; Cho W-S; Choi N; Parvizi J; Kim T How accurate are orthopedic surgeons in diagnosing periprosthetic joint infection after total knee arthroplasty?: A multicenter study. Knee 2015, 22, 180–185. [PubMed: 25728568]

(192). Berbari EF; Hanssen AD; Duffy MC; Steckelberg JM; Ilstrup DM; Harmsen WS; Osmon DR Risk factors for prosthetic joint infection: case-control study. Clin. Infect. Dis 1998, 27, 1247–1254. [PubMed: 9827278]

(193). Zmistowski B; Restrepo C; Huang R; Hozack W; Parvizi J Periprosthetic joint infection diagnosis – A complete understanding of white blood cell count and differential. J. Arthroplasty 2012, 27, 1589–1593. [PubMed: 22543180]

(194). Parvizi J; Gehrke T Definition of periprosthetic joint infection. J. Arthroplasty 2014, 29, 1331. [PubMed: 24768547]

(195). Neumann D; Hofstaedter T; List C; Dorn U Two-stage cementless revision of late total hip arthroplasty infection using a premanufactured spacer. J. Arthroplasty 2012, 27, 1397–1401. [PubMed: 22177795]

(196). Beckmann J; Kees F; Schaumburger J; Kalteis T; Lehn N; Grifka J; Lerch K Tissue concentrations of vancomycin and Moxifloxacin in periprosthetic infection in rats. Acta Orthop 2007, 78, 766–773. [PubMed: 18236182]

(197). Mistry S; Roy S; Maitra NJ; Kundu B; Chanda A; Datta S; Joy M A novel, multi-barrier, drug eluting calcium sulfate/biphasic calcium phosphate biodegradable composite bone cement for treatment of experimental MRSA osteomyelitis in rabbit model. J. Controlled Release 2016, 239, 169–181.

(198). Ford CA; Spoonmore TJ; Gupta MK; Duvall CL; Guelcher SA; Cassat JE Diflunisal-loaded poly(propylene sulfide) nanoparticles decrease S. aureus-mediated bone destruction during osteomyelitis. J. Orthop. Res 2021, 39, 426–437. [PubMed: 33300149]

(199). Seyednejad H; Gawlitta D; Kuiper RV; de Bruin A; van Nostrum CF; Vermonden T; Dhert WJA; Hennink WE In vivo biocompatibility and biodegradation of 3D-printed porous scaffolds based on a hydroxyl-functionalized poly(ε-caprolactone). Biomaterials 2012, 33, 4309–4318. [PubMed: 22436798]

(200). Cui X; Huang C; Zhang M; Ruan C; Peng S; Li L; Liu W; Wang T; Li B; Huang W; Rahaman MN; Lu WW; Pan H Enhanced osteointegration of poly(methylmethacrylate) bone cements by incorporating strontium-containing borate bioactive glass. J. R. Soc., Interface 2017, 14, 20161057. [PubMed: 28615491]

(201). ASTM. F451–21 Standard Specification for Acrylic Bone Cement ASTM International, 2021.

(202). ISO. 5833:2002 Implants for surgery – Acrylic resin cements International Organization for Standardization, 2002.

(203). Jones M; Buckle C How does aseptic loosening occur and how can we prevent it? Orthop. Trauma 2020, 34, 146–152.

(204). Huang D; Niu L; Wei Y; Guo M; Zuo Y; Zou Q; Hu Y; Chen W; Li Y Interfacial and biological properties of the gradient coating on polyamide substrate for bone substitute. J. R. Soc., Interface 2014, 11, 20140101. [PubMed: 25121648]

(205). Netti PA; Shelton JC; Revell PA; Pirie C; Smith S; Ambrosio L; Nicolais L; Bonfield W Hydrogels as an interface between bone and an implant. Biomaterials 1993, 14, 1098–1104. [PubMed: 8312463]

(206). Link D; van den Dolder J; van den Beucken J; Wolke J; Mikos A; Jansen J Bone response and mechanical strength of rabbit femoral defects filled with injectable CaP cements containing TGF-beta1 loaded gelatin microparticles. Biomaterials 2008, 29, 675–682. [PubMed: 17996293]

(207). Fukuda C; Goto K; Imamura M; Neo M; Nakamura T Bone bonding ability and handling properties of a titaniapolymethylmethacrylate (PMMA) composite bioactive bone cement modifies with a unique PMMA powder. Acta Biomater 2011, 7, 3595–3600. [PubMed: 21704200]

(208). Erhart S; Schmoelz W; Blauth M; Lenich A Biomechanical effect of bone cement augmentation on rotational stability and pull-out strength of the proximal femur nail antirotation-TM. Injury 2011, 42, 1322–1327. [PubMed: 21601203]

(209). Funk M; Litsky A Effect of cement modulus on the shear properties of the bone-cement interface. Biomaterials 1998, 19, 1561–1567. [PubMed: 9830981]

(210). Park K; Park J Interfacial strength of compression-molded specimens between PMMA powder and PMMA/MMA monomer solution-treated ultra-high molecular weight polyethylene (UHMWPE) powder. J. Biomed. Mater. Res 2000, 53, 737–747. [PubMed: 11074434]

(211). Lee C The mechanical properties of PMMA bone cement. In The well-cemented total hip arthroplasty; Breusch S, Malchau H, Eds.; Springer: Berlin, Heidelberg, 2005; pp 60–66.

(212). Wancket L Animal models for evaluation of bone implants and devices: comparative bone structure and common model uses. Vet. Pathol 2015, 52, 842–850. [PubMed: 26163303]

(213). Raina D; Larsson D; Sezgin E; Isaksson H; Tagil M; Lidgren L Biomodulation of an implant for enhanced bone-implant anchorage. Acta Biomater 2019, 96, 619–630. [PubMed: 31301423]

(214). Geng T; Chen X; Zheng M; Yu H; Zhang S; Sun S; Guo H; Jin Q Effects of strontium ranelate on wear particle-induced aseptic loosening in female ovariectomized mice. Mol. Med. Rep 2018, 18, 1849–1857. [PubMed: 29901109]

(215). Vertesich K; Sosa BR; Niu Y; Ji G; Suhardi V; Turajane K; Mun S; Xu R; Windhager R; Park-Min KH; Greenblatt MB; Bostrom MP; Yang X Alendronate enhances osseointegration in a murine implant model. J. Orthop. Res 2021, 39, 719–726. [PubMed: 32915488]

(216). Zhao T; Guo W; Yin Y; Tan Y Bolt pull-out tests of anchorage body under different loading rates. Shock Vib 2015, 2015, 121673.

(217). Burr DB; Gallant MA Bone remodeling in osteoarthritis. Nat. Rev. Rheumatol 2012, 8, 665–673. [PubMed: 22868925]

(218). Sanches CP; Vianna AGD; de Carvalho Barreto F The impact of type 2 diabetes on bone metabolism. Diabetol. Metab. Syndr 2017, 9, 85. [PubMed: 29075333]

(219). Ingham E; Fisher J The role of macrophages in osteolysis of total joint replacement. Biomaterials 2005, 26, 1271–1286. [PubMed: 15475057]

(220). Kepler CK; Nho SJ; Bansal M; Ala OL; Craig EV; Wright TM; Warren RF Radiographic and histopathologic analysis of osteolysis after total shoulder arthroplasty. J. Shoulder Elbow Surg 2010, 19, 588–595. [PubMed: 20036583]

(221). Kaur S; Harjai K; Chhibber S In vivo assessment of phage and linezolid based implant coatings for treatment of methicillin resistant S. aureus (MRSA) mediated orthopaedic device related infections. PLoS One 2016, 11, e0157626. [PubMed: 27333300]

(222). Hu C-C; Chang C-H; Chang Y; Hsieh J-H; Ueng SW-N Beneficial effect of TaON-Ag nanocomposite titanium on antibacterial capacity in orthopedic application. Int. J. Nanomed 2020, 15, 7889–7900.

(223). Jiang Y; Wang S-N; Wu H-T; Qin H-J; Ren M-L; Lin J-C; Yu B Aspirin alleviates orthopedic implant-associated infection. Int. J. Mol. Med 2019, 44, 1281–1288. [PubMed: 31432131]

(224). Wang R; Shi M; Xu F; Qiu Y; Zhang P; Shen K; Zhao Q; Yu J; Zhang Y Graphdiyne-modified TiO_2 nanofibers with osteoinductive and enhanced photocatalytic antibacterial activities to prevent implant infection. Nat. Commun 2020, 11, 4465. [PubMed: 32901012]

(225). Zhou W; Peng X; Ma Y; Hu Y; Wu Y; Lan F; Weir MD; Li M; Ren B; Oates TW; Xu HHK; Zhou X; Cheng L Two-staged time-dependent materials for the prevention of implant-related infections. Acta Biomater 2020, 101, 128–140. [PubMed: 31629895]

(226). Li Y; Liu G; Zhai Z; Liu L; Li H; Yang K; Tan L; Wan P; Liu X; Ouyang Z; Yu Z; Tang T; Zhu Z; Qu X; Dai K Antibacterial properties of magnesium in vitro and in an in vivo model of implant-associated methicillin-resistant Staphylococcus aureus infection. Antimicrob. Agents Chemother 2014, 58, 7586–7591. [PubMed: 25288077]

(227). Ding Y; Hao Y; Yuan Z; Tao B; Chen M; Lin C; Liu P; Cai K A dual-functional implant with an enzyme-responsive effect for bacterial infection therapy and tissue regeneration. Biomater. Sci 2020, 8, 1840–1854. [PubMed: 31967110]

(228). Folsch C; Federmann M; Kuehn KD; Kittinger C; Kogler S; Zarfel G; Kerwat M; Braun S; Fuchs-Winkelmann S; Paletta JRJ; Roessler PP Coating with a novel gentamicinpalmitate formulation prevents implant-associated osteomyelitis induced by methicillin-susceptible Staphylococcus aureus in a rat model. Int. Orthop 2015, 39, 981–988. [PubMed: 25380688]

(229). Diefenbeck M; Schrader C; Gras F; Muckley T; Schmidt J; Zankovych S; Bossert J; Jandt KD; Volpel A; Sigusch BW; Schubert H; Bischoff S; Pfister W; Edel B; Faucon M; Finger U Gentamicin coating of plasma chemical oxidized titanium alloy prevents implant-related osteomyelitis in rats. Biomaterials 2016, 101, 156–164. [PubMed: 27294535]

(230). Yang Z; Xi Y; Bai J; Jiang Z; Wang S; Zhang H; Dai W; Chen C; Gou Z; Yang G; Gao C Covalent grafting of hyperbranched poly-L-lysine on Ti-based implants achieves dual functions of antibacterial and promoted osteointegration in vivo. Biomaterials 2021, 269, 120534. [PubMed: 33243425]

(231). Yang Y; Ao H-Y; Yang S-B; Wang Y-G; Lin W-T; Yu Z-F; Tang T-T In vivo evaluation of the anti-infection potential of gentamicin-loaded nanotubes on titania implants. Int. J. Nanomed 2016, 11, 2223–2234.

(232). Shen J; Gao P; Han S; Kao RYT; Wu S; Liu X; Qian S; Chu PK; Cheung KMC; Yeung KWK A tailored positively-charged hydrophobic surface reduces the risk of implant associated infections. Acta Biomater 2020, 114, 421–430. [PubMed: 32711080]

(233). Gao Z; Song M; Liu R-L; Shen Y; Ward L; Cole I; Chen X-B; Liu X Improving in vitro and in vivo antibacterial functionality of Mg alloys through micro-alloying with Sr and Ga. Mater. Sci. Eng., C 2019, 104, 109926.

(234). Harrasser N; Gorkotte J; Obermeier A; Feihl S; Straub M; Slotta-Huspenina J; von Eisenhart-Rothe R; Moser W; Gruner P; de Wild M; Gollwitzer H; Burgkart R A new model of implant-related osteomyelitis in the metaphysis of rat tibiae. BMC Musculoskeletal Disord 2016, 17, 152.

(235). Cao Z; Jiang D; Yan L; Wu J In vitro and in vivo drug release and antibacterial properties of the novel vancomycin-loaded bone-like hydroxyapatite/poly amino acid scaffold. Int. J. Nanomed 2017, 12, 1841–1851.

(236). Moojen DJF; Vogely HC; Fleer A; Nikkels PGJ; Higham PA; Verbout AJ; Castelein RM; Dhert WJA Prophylaxis of infection and effects on osseointegration using a tobramycin-periapatite coating on titanium implants – an experimental study in the rabbit. J. Orthop. Res 2009, 27, 710–716. [PubMed: 19025776]

(237). Metsemakers WJ; Schmid T; Zeiter S; Ernst M; Keller I; Cosmelli N; Arens D; Moriarty TF; Richards RG Titanium and steel fracture fixation plates with different surface topographies: influence on infection rate in a rabbit fracture model. Injury 2016, 47, 633–639. [PubMed: 26830128]

(238). Chen J; Hu G; Li T; Chen Y; Gao M; Li Q; Hao L; Jia Y; Wang L; Wang Y Fusion peptide engineered “statically-versatile” titanium implant simultaneously enhancing anti-infection, vascularization and osseointegration. Biomaterials 2021, 264, 120446. [PubMed: 33069134]

(239). Yuan Z; Tao B; He Y; Liu J; Lin C; Shen X; Ding Y; Yu Y; Mu C; Liu P; Cai K Biocompatible Mo/PDA-RGD coating on titanium implant with antibacterial property via intrinsic ROS-independent oxidative stress and NIR irradiation. Biomaterials 2019, 217, 119290. [PubMed: 31252244]

(240). Radwan NH; Nasr M; Ishak RA; Abdeltawab NF; Awad GA Chitosan-calcium phosphate composite scaffolds for control of post-operative osteomyelitis: fabrication, characterization, and in vitro-in vivo evaluation. Carbohydr. Polym 2020, 244, 116482. [PubMed: 32536391]

(241). Gimeno M; Pinczowski P; Mendoza G; Asin J; Vazquez FJ; Vispe E; Garcia-Alvarez F; Perez M; Santamaria J; Arruebo M; Lujan L Antibiotic-eluting orthopedic device to prevent early implant associated infections: efficacy, biocompatibility and biodistribution studies in an ovine model. J. Biomed. Mater. Res., Part B 2018, 106, 1976–1986.

(242). Gimeno M; Pinczowski P; Vazquez FJ; Perez M; Santamaria J; Arruebo M; Lujan L Porous orthopedic steel implant as an antibiotic eluting device: prevention of post-surgical infection on an ovine model. Int. J. Pharm 2013, 452, 166–172. [PubMed: 23651643]

(243). Williams DL; Epperson RT; Ashton NN; Taylor NB; Kawaguchi B; Olsen RE; Haussener TJ; Sebahar PR; Allyn G; Looper RE In vivo analysis of a first-in-class tri-alkyl norspermidine-biaryl antibiotic in an active release coating to reduce the risk of implant-related infection. Acta Biomater 2019, 93, 36–49. [PubMed: 30710710]

(244). Stewart S; Barr S; Engiles J; Hickok NJ; Shapiro IM; Richardson DW; Parvizi J; Schaer TP Vancomycin-modified implant surface inhibits biofilm formation and supports bone-healing in an infected osteotomy model in sheep: a proof-of-concept study. J. Bone Joint Surg. Am 2012, 94, 1406–1415. [PubMed: 22854994]

(245). Tran N; Tran PA; Jarrell JD; Engiles JB; Thomas NP; Young MD; Hayda RA; Born CT In vivo caprine model for osteomyelitis and evaluation of biofilm-resistant intramedullary nails. BioMed Res. Int 2013, 2013, 674378. [PubMed: 23841085]

(246). Cao H; Qin H; Zhao Y; Jin G; Lu T; Meng F; Zhang X; Liu X Nano-thick calcium oxide armed titanium: boosts bone cells against methicillin-resistant Staphylococcus aureus. Sci. Rep 2016, 6, 21761. [PubMed: 26899567]

(247). Oezel L; Buren C; Scholz AO; Windolf J; Windolf CD Effect of antibiotic infused calcium sulfate/hydroxyapatite (CAS/HA) insets on implant-associated osteitis in a femur fracture model in mice. PLoS One 2019, 14, e0213590. [PubMed: 30870491]

(248). Tomizawa T; Nishitani K; Ito H; Okae Y; Morita Y; Doi K; Saito M; Ishie S; Yoshida S; Murata K; Yoshitomi H; Kuroda Y; Matsuda S The limitations of mono- and combination antibiotic therapies on immature biofilms in a murine model of implant-associate osteomyelitis. J. Orthop. Res 2021, 39, 449–457. [PubMed: 33325059]

(249). Thompson JM; Saini V; Ashbaugh AG; Miller RJ; Ordonez AA; Ortines RV; Wang Y; Sterling RS; Jain SK; Miller LS Oral-only linezolid-rifampin is highly effective compared with other antibiotics for periprosthetic joint infection: study of a mouse model. J. Bone Joint Surg. Am 2017, 99, 656–665. [PubMed: 28419033]

(250). Kussmann M; Obermueller M; Berndl F; Reischer V; Veletzky L; Burgmann H; Poeppl W Dalbavancin for treatment of implant-related methicillin-resistant Staphylococcus aureus osteomyelitis in an experimental rat model. Sci. Rep 2018, 8, 9661. [PubMed: 29941909]

(251). Sethi S; Thormann U; Sommer U; Stotzel S; Mohamed W; Schnettler R; Domann E; Chakraborty T; Alt V Impact of prophylactic CpG oligodeoxynucleotide application on implant-associated Staphylococcus aureus bone infection. Bone 2015, 78, 194–202. [PubMed: 25959416]

(252). Kemah B; Uzer G; Turhan Y; Ozturan B; Kilic B; Gultepe BS; Ceyran AB; Erturk S; Aksoylu B; Senaydin O; Ozkan K Effects of local application of nano-silver on osteomyelitis and soft tissue infections: an experimental study in rats. J. Bone Jt. Infect 2018, 3, 43–49. [PubMed: 29774178]

(253). Greimel F; Scheuerer C; Gessner A; Simon M; Kalteis T; Grifka J; Benditz A; Springorum H-R; Schaumburger J Efficacy of antibiotic treatment of implant-associated Staphylococcus aureus infections with moxifloxacin, flucloxacillin, rifampin, and combination therapy: an animal study. Drug Des., Dev. Ther 2017, 11, 1729–1736.

(254). Kalteis T; Beckmann J; Schroder H-J; Schaumburger J; Linde H-J; Lerch K; Lehn N Treatment of implant-associated infections with moxifloxacin: an animal study. Int. J. Antimicrob. Agents 2006, 27, 444–448. [PubMed: 16621461]

(255). Liu Y; Bai X; A L In vitro and in vivo evaluation of a ciprofloxacin delivery system based on poly(DLLA-co-GA-co-CL) for treatment of chronic osteomyelitis. J. Appl. Biomater. Funct. Mater 2020, 18, 1–13.

(256). Saleh-Mghir A; Muller-Serieys C; Dinh A; Massias L; Cremieux A-C Adjuctive rifampin is crucial to optimizing daptomycin efficacy against rabbit prosthetic joint infection due to methicillin-resistant Staphylococcus aureus. Antimicrob. Agents Chemother 2011, 55, 4589–4593. [PubMed: 21825285]

(257). Gatin L; Saleh-Mghir A; Tasse J; Ghout I; Laurent F; Cremieux A-C Ceftaroline-fosamil efficacy against methicillin-resistant Staphylococcus aureus in a rabbit prosthetic joint infection model. Antimicrob. Agents Chemother 2014, 58, 6496–6500. [PubMed: 25136014]

(258). Nandi SK; Shivaram A; Bose S; Bandyopadhyay A Silver nanoparticle deposited implants to treat osteomyelitis. J. Biomed. Mater. Res., Part B 2018, 106, 1073–1083.

(259). Huneault LM; Lussier B; Dubreuil P; Chouinard L; Desevaux C Prevention and treatment of experimental osteomyelitis in dogs with ciprofloxacin-loaded crosslinked high amylose starch implants. J. Orthop. Res 2004, 22, 1351–1357. [PubMed: 15475220]

(260). Neyisci C; Erdem Y; Bilekli AB; Demiralp B; Kose O; Bek D; Korkusuz F; Kankilic B Treatment of implant-related methicillin-resistant Staphylococcus aureus osteomyelitis with vancomycin-loaded VK100 silicone cement: an experimental study in rats. J. Orthop. Surg. (Hong Kong) 2018, 26, 1–10.

(261). Jain K; Vedarajan R; Watanabe M; Ishikiriyama M; Matsumi N Tunable LCST behavior of poly(N-isopropylacrylamide/ionic liquid) copolymers. Polym. Chem 2015, 6, 6819–6825.

(262). Grinberg VY; Burova TV; Grinberg NV; Tikhonov VE; Dubovik AS; Moskalets AP; Khokhlov AR Thermodynamic insight into the thermoresponsive behavior of chitosan in aqueous solutions: a differential scanning calorimetry study. Carbohydr. Polym 2020, 229, 115558. [PubMed: 31826515]

(263). Ehrensberger MT; Tobias ME; Nodzo SR; Hansen LA; Luke-Marshall NR; Cole RF; Wild LM; Campagnari AA Cathodic voltage-controlled electrical stimulation of titanium implants as treatment for methicillin-resistant Staphylococcus aureus peri-prosthetic infections. Biomaterials 2015, 41, 97–105. [PubMed: 25522969]

(264). Murr L Metallurgy principles applied to powder bed fusion 3D printing/additive manufacturing of personalized and optimized metal and allow biomedical implants: an overview. J. Mater. Res. Technol 2020, 9, 1087–1103.

(265). Oladapo B; Ismail S; Bowoto O; Omigbodun F; Olawumi M; Muhammad M Lattice design and 3D-printing of PEEK with $Ca_{10}(OH)(PO_4)_3$ and in-vitro bio-composite for bone implant. Int. J. Biol. Macromol 2020, 165, 50–62. [PubMed: 32979443]

(266). Schwarz EM; Parvizi J; Gehrke T; Aiyer A; Battenberg A; Brown SA; Callaghan JJ; Citak M; Egol K; Garrigues GE; Ghert M; Goswami K; Green A; Hammound S; Kates SL; McLaren AC; Mont MA; Namdari S; Obremskey WT; O'Toole R; Raikin S; Restrepo C; Ricciardi B; Saeed K; Sanchez-Sotelo J; Shohat N; Tan T; Thirukumaran CP; Winters B 2018 International consensus meeting on musculoskeletal infection: research priorities from the general assembly questions. J. Orthop. Res 2019, 37, 997–1006. [PubMed: 30977537]

(267). BioRender, 2021. https://biorender.com (accessed 2021-06-20).

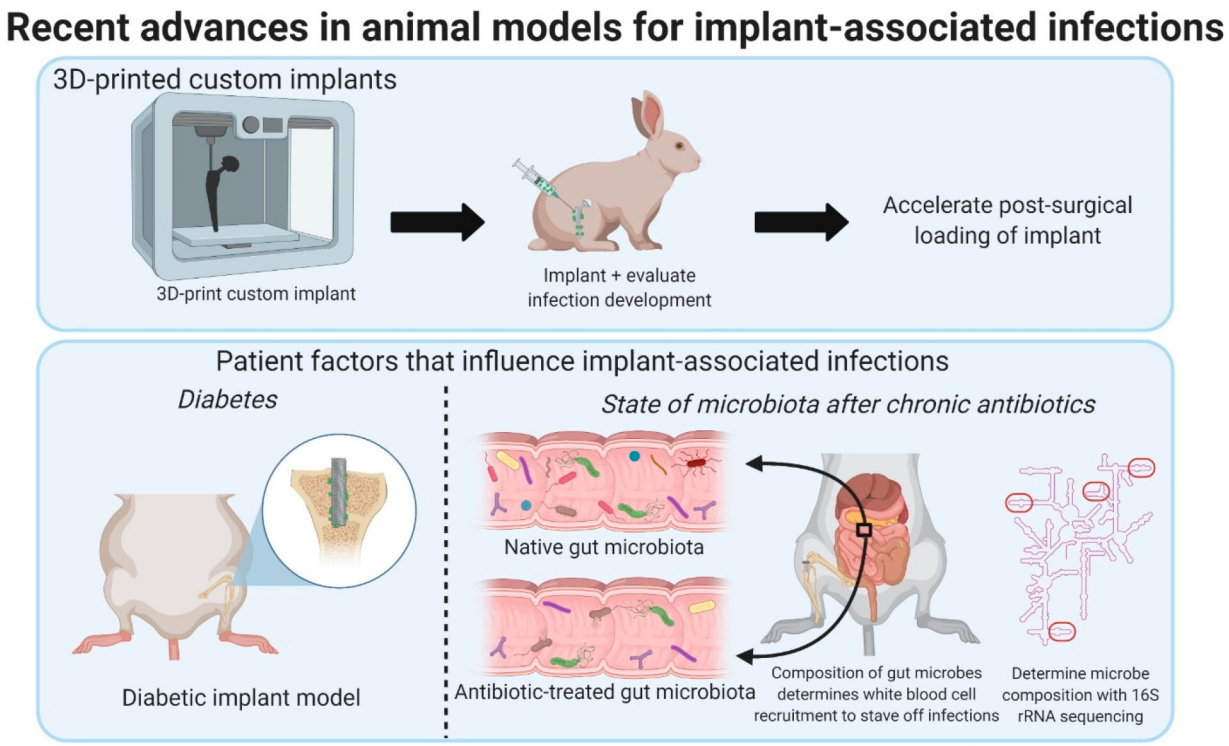

Figure 1.

Summary of recent advances in implant-associated infection preclinical *in vivo* models used to simulate the clinical environment of infections. Models have utilized emerging technologies of 3D-printing and bacterial genomic sequencing to improve the clinical relevancy of the model and to analyze the role of patient risk factors on the development of implant-associated infections. Figure created using BioRender.com.[267]

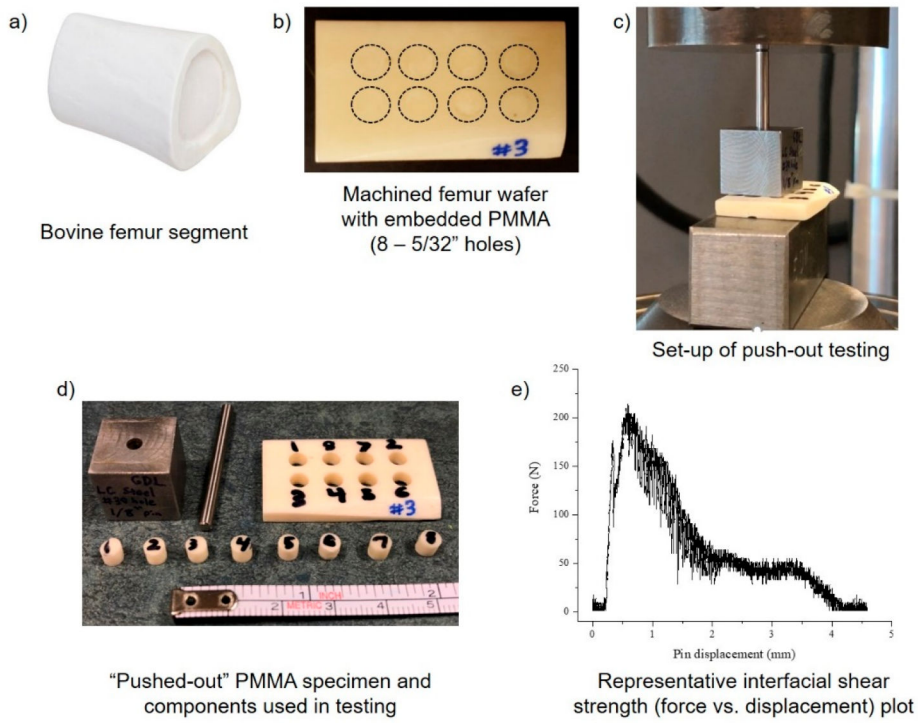

Figure 2.

Setup of *ex vivo* PMMA bone cement push-out testing model using bovine femur tissue. Small, uniform wafers of bovine femur were machined from a cleaned/bleached femur segment (a) with eight 5/32 in. holes spaced 0.3 in. apart (b). Holes in the femur wafer were packed with PMMA materials, and a 1/8 in. steel pin was used to push embedded PMMA out of the femur wafer under compressive force at a loading rate of 20 mm/min (c). "Pushed-out" PMMA specimen from femur wafer (d). Representative raw force versus displacement plot of interfacial shear strength of PMMA pushed-out of a single 5/32 in. hole (e). Images were taken by the authors.

Table 1.

Summary of Advantages and Limitations of Metallic Antimicrobial Biomaterials from the Past Decade Designed for Orthopedic Implant-Associated Infection Applications

metals					
composition	**tested *in vivo?***	**antimicrobial activity**	**advantages**	**limitations**	**ref**
titanium oxide nanocoating on titanium	no	bacterial clearance of 80–90% CFUs, inhibit adhesion 80% bacteria	(1) intrinsic activity	(1) leach metal particles (cytotoxicity/genotoxicity)	49, 50
			(2) long-lasting		
			(3) decreased resistance		
titanium oxide coated titanium and titanium hydride powder coated on porous titanium	no	inhibit adhesion 80% bacteria	(1) intrinsic activity	(1) leach metal particles (cytotoxicity/genotoxicity)	51
			(2) long-lasting		
			(3) decreased resistance		
silver and copper nanoparticle coated titanium oxide on Ti6Al4V	no	inhibit adhesion 100% bacteria	(1) intrinsic activity	(1) leach metal particles (cytotoxicity/genotoxicity)	52
			(2) long-lasting		
			(3) decreased resistance		
silver and zinc nanoparticle coated titanium oxide on Ti6Al4V	no	inhibit adhesion 100% bacteria	(1) intrinsic activity	(1) leach metal particles (cytotoxicity/genotoxicity)	53
			(2) long-lasting		
			(3) promotes osseointegration		
titanium–copper-oxide coated Ti6Al4V	no	2log10 decrease in bacterial adhesion	(1) intrinsic activity	(1) leach metal particles (cytotoxicity/genotoxicity)	56
			(2) long-lasting		
fluorine- and phosphorus doped nanostructured Ti6Al4V	yes	not evaluated, used to detect presence of infection	(1) intrinsic activity	(1) leach metal particles (cytotoxicity/genotoxicity)	40
			(2) long-lasting		
			(3) promotes osseointegration		
magnesium alloy	yes	limited *in vivo*, requires modification	(1) intrinsic activity	(1) limited duration of activity	59
				(2) antimicrobial activity *in vitro* superior to *in vivo*	

Table 2.

Summary of Advantages and Limitations of Polymeric Antimicrobial Biomaterials from the Past Decade Designed for Orthopedic Implant-Associated Infection Applications

polymers: natural and synthetic					
composition	**tested *in vivo*?**	**antimicrobial activity**	**advantages**	**limitations**	**ref**
chitosan sponges	yes	7–21 days activity zone of inhibition	(1) tunable delivery kinetics (2) intrinsic activity (3) biocompatibility	(1) may require antibiotic supplement (2) limited duration of activity	83
collagen sponges	yes	3–4log10 decrease bacterial CFUs	(1) biocompatibility	(1) require antibiotics (2) limited duration of activity	86
poly(lactic acid) diol and poly(caprolactone) diol coated polyethylene terephthalate	yes	up to 66 days activity (*in vitro*) and 20 days activity (*in vivo*) zone of inhibition	(1) tunable delivery kinetics	(1) require antibiotics (2) limited duration of activity	87
poly(L-lactic)acid coated poly(D,L-lactide-*co*-lactide)	no	not evaluated	(1) tunable delivery kinetics	(1) require antibiotics (2) limited duration of activity	88
poly(D-L-lactide) coating	no	inhibit adhesion 60% bacteria	(1) tunable delivery kinetics	(1) require antibiotics (2) limited duration of activity	89
micropatterned silicone	yes	inhibit adhesion of >90% bacteria	(1) intrinsic activity (2) long-lasting	(1) short range of antimicrobial action (only prevent bacterial attachment to surface)	41
xerogel coating (silane-based) on silicone	yes	82% reduction implant infection (*in vivo*)	(1) intrinsic activity	(1) limited duration of activity	135
sulfonated poly(ether ether ketone)	yes	bacterial clearance of 80–100% CFUs	(1) promote osteogenesis (2) durability	(1) limited duration of activity	112
cross-linked PEG	yes	bacterial clearance of 100% CFUs	(1) injectable (minimally invasive application)	(1) limited duration of activity	120
poly (ethylene imine)/poly(sodium-4-styrenesulfonate)/poly(allylamine hydrochloride)	no	inhibit adhesion 80% bacteria	(1) local drug synthesis	(1) cytotoxicity of poly(ethylenimine)	121

Table 3.

Summary of Advantages and Limitations of Ceramic Antimicrobial Biomaterials from the Past Decade Designed for Orthopedic Implant-Associated Infection Applications

ceramics					
composition	**tested *in vivo*?**	**antimicrobial activity**	**advantages**	**limitations**	**ref**
calcium sulfate (dihydrate/hemihydrate)	yes	not evaluated	(1) promote osseointegration	(1) require antibiotics (2) limited duration of activity	141–143
biphasic nanohydroxyapatite/calcium sulfate	yes	bacterial clearance of 100% CFUs	(1) promote osseointegration	(1) require antibiotics (2) Limited duration of activity	144
β-tricalcium phosphate/calcium sulfate	no	5–40 days activity zone of inhibition (*in vitro*)	(1) promote osseointegration	(1) require antibiotics (2) limited duration of activity	145

Table 4.

Summary of Advantages and Limitations of Composite Antimicrobial Biomaterials from the Past Decade Designed for Orthopedic Implant-Associated Infection Applications

combination materials/composites					
composition	**tested *in vivo*?**	**antimicrobial activity**	**advantages**	**limitations**	**ref**
zirconium nitride coated ceramic covered Co–Cr–Mo	no	log10 decrease bacterial CFUs	(1) intrinsic activity	(1) short range of antimicrobial action (only prevent bacterial attachment to surface)	149
			(2) long-lasting		
Titanium–niobium-nitride coated titanium	no	4-fold decrease in bacterial adhesion	(1) intrinsic activity	(1) leach metal particles (cytotoxicity/genotoxicity)	159
			(2) long-lasting		
nanostructured silver-substituted fluorhydroxyapatite-titanium oxide coated titanium	no	bacterial clearance of 100% CFUs	(1) intrinsic activity	(1) leach metal particles (cytotoxicity/genotoxicity)	146
			(2) long-lasting		
			(3) promote osseointegration		
carboxymethyl chitosan/hyaluronic-acid-catechol conjugated vascular endothelial growth factor functionalized titanium	no	inhibit adhesion of 46–84% bacteria	(1) intrinsic activity	(1) short range of antimicrobial action (only prevent bacterial attachment to surface)	160
			(2) promotes osseointegration		
zinc, cerium, selenium substituted hydroxyapatite/poly(sorbitol sebacate glutamate) coated titanium	yes	1 day activity zone of inhibition (*in vitro*)	(1) intrinsic activity	(1) leach metal particles (cytotoxicity/genotoxicity)	147
			(2) promotes osseointegration		
silver hydroxyapatite coating on titanium	yes	10–20% decrease in bacterial biofilm adhesion	(1) intrinsic activity	(1) leach metal particles (cytotoxicity/genotoxicity)	148
			(2) long-lasting		
			(3) promotes osseointegration		
silver doped nano calcium phosphate coated Ti6Al4V	yes	significant reduction in bacterial adhesion relative to controls	(1) intrinsic activity	(1) leach metal particles (cytotoxicity/genotoxicity)	157
			(2) long-lasting		
			(3) promotes osseointegration		
Eudragit coated Ti6Al4V	yes	15 days activity zone of inhibition (*in vitro*)	(1) pH-triggered drug delivery	(1) require antibiotics	161
				(2) limited duration of activity	

combination materials/composites					
composition	**tested *in vivo*?**	**antimicrobial activity**	**advantages**	**limitations**	**ref**
mesoporous silica microparticles in porous stainless steel	no	2–3log10 decrease in bacterial adhesion	(1) tunable drug delivery properties	(1) require antibiotics (2) limited duration of activity	162
copper-nanoparticle coated sulfonated poly(ether ether ketone)	yes	35-fold decrease in bacterial adhesion	(1) intrinsic activity (2) long-lasting	(1) leach metal particles (cytotoxicity/ genotoxicity)	114
cationic liposomes in calcium sulfate	yes	bacterial clearance of 100% CFUs	(1) promote osseointegration	(1) require antibiotics (2) limited duration of activity	28
chitosan bonded borate bioglass particles	yes	81–87% clearance of infection *in vivo*	(1) promotes osseointegration (2) injectable	(1) require antibiotics (2) limited duration of activity	30
brushite calcium phosphate functionalized poly(ether ether ketone)	Yes	inhibit adhesion 100% bacteria	(1) promotes osseointegration	(1) require antibiotics (2) limited duration of activity	113
cyclodextrin microparticles in PMMA	No	10–60 days activity zone of inhibition (*in vitro*)	(1) can be repeatedly filled with drug locally (2) unaffected by bacterial biofilm	(1) require antibiotics	29, 123–125

ACS Infect Dis. Author manuscript; available in PMC 2022 November 28.

Table 5.

Summary of Preclinical *In Vivo* Models from the Past Decade Used to Establish and Study Implant-Associated Infections

models to establish and study implant infections						
animal model	**implant/location**	**pathogen**	**study duration**	**key evaluation**	**summary**	**ref**
fish – zebrafish	none	*S. aureus* SH1000-derived	3 weeks	(1) histology	bone fracture model in zebrafish	169
		2.5×10^9 CFU		(2) confocal imaging		
mice – BALB/C	titanium in femur	*S. aureus* ATCC 29213	4 weeks	(1) CFU count	model to study implant infection biofilms	170
		2×10^3–5×10^6 CFU		(2) collect blood		
				(3) X-rays		
				(4) SEM biofilm		
				(5) histology		
mice – BALB/C	titanium in femur	*S.aureus* ATCC 29213	4 weeks	(1) CFU count	model for histology scores of implant infection	171
		1×10^3 CFU		(2) X-rays		
				(3) histology		
mice – BALB/C	stainless steel in tibia	*S. aureus* USA300	2 weeks	(1) CFU count	first animal model of *S. agalactiae* implant infection	172
		5×10^5 CFU		(2) micro-CT		
		S. agalactiae COH1		(3) histology		
		5×10^5 CFU		(4) TRAP quantify		
mice – diabetic NOD/ShiLtJ CD1	stainless steel in femur	*S. aureus* ATCC 25923	4 weeks	(1) CFU count	diabetic model of implant infection	32
		1×10^3 CFU		(2) collect blood		
				(3) micro-CT		
				(4) SEM biofilm		
				(5) histology		
mice – C57BL/6 and BALB/C	titanium or poly(ether ether ketone) in femur	*S. aureus* JAR 06.01.31	1 week	(1) CFU count	influence of implant material on implant infection	115
		9×10^5 CFU		(2) histology		
mice – C57BL/6	titanium in femur	*P. aeruginosa* Xen 41	3 weeks	(1) CFU count	Gram-negative implant infection model	163
		1×10^3–1×10^5 CFU		(2) X-rays		
		E. coli Xen 14		(3) histology		
		1×10^3–1×10^5 CFU		(4) *In vivo* BLI		

ACS Infect Dis. Author manuscript; available in PMC 2022 November 28.

models to establish and study implant infections						
animal model	**implant/location**	**pathogen**	**study duration**	**key evaluation**	**summary**	**ref**
				(5) PET imaging		
				(6) Flow cytometry		
mice – C57BL/6	Ti6Al4V in tibia	*S. aureus* Xen 36	2 and 6 weeks	(1) CFU count	clinically relevant load-bearing model of periprosthetic joint infection	173
		3×10^5 CFU		(2) collect blood		
				(3) X-rays		
				(3) SEM biofilm		
				(4) gait analysis		
mice – C57BL/6	titanium in tibia	*S. aureus* Xen 36	12 weeks, disrupt microbiota	(1) CFU count	role of the gut microbiota on periprosthetic joint infection	33
		1×10^2 CFU		(2) collect blood		
				(3) X-rays		
			5 days, postsurgery	(4) gait analysis		
				(5) bacterial sequencing		
mice – C57BL/6	stainless steel in humerus	*S. aureus* Xen 36	6 weeks	(1) CFU count	model of implant infection in humerus	174
		1×10^3 CFU		(2) X-ray		
				(3) histology		
				(4) *in vivo* BLI		
mice – C57BL/6	stainless steel in tibia	*S. aureus* Xen 40	2 weeks	(1) CFU count	quantitative model of implant biofilm	175
				(2) SEM biofilm		
				(3) *in vivo* BLI		
rats – Sprague–Dawley	Ti6Al4V in tibia	*S. aureus* ATCC 25923	6 weeks	(1) CFU count	model of implant infection in metaphysis	176
		1×10^3–1×10^6 CFU		(2) collect blood		
				(3) X-rays		
				(4) histology		
rats – Sprague–Dawley	stainless steel in tibia	*S. aureus* ATCC 49230	4 weeks	(1) CFU count	model of implant infection dependent on bacterial inoculation	177
		1×10^2–1×10^6 CFU		(2) collect blood		
				(3) X-rays		

ACS Infect Dis. Author manuscript; available in PMC 2022 November 28.

models to establish and study implant infections						
animal model	**implant/location**	**pathogen**	**study duration**	**key evaluation**	**summary**	**ref**
				(4) histology		
rats – Sprague–Dawley	metal alloy and high density poly ethylene in femur/tibia	*S. aureus* clinical MN8 and UAMS-1	6 weeks	(1) CFU count	model of knee implant infection	178
		1×10^2–1×10^4 CFU		(2) collect blood		
				(3) X-rays		
				(4) histology		
rats – Sprague–Dawley	titanium in femur	*S. aureus* ATCC 49230	6 weeks	(1) CFU count	model of implant infection, hematogenous osteomyelitis complication	12
		1×10^4–1×10^9 CFU		(2) micro-CT		
				(3) histology		
rats – Sprague–Dawley	titanium and ultrahigh molecular weight polyethylene in tibia/ femur	*S. aureus* Xen 29	4 weeks	(1) CFU count	longitudinal infection model with two implant components that enables monitoring of postsurgery recovery	179
		2×10^7 CFU		(2) X-rays		
				(3) micro-CT		
				(4) collect blood		
				(5) histology		
				(6) gait analysis		
rats – Sprague–Dawley	3D printed Ti6Al4V + PMMA in tibia	*S. aureus* ORI16_C02N	4 weeks	(1) CFU count	model of knee implant infection	128
		2×10^4 CFU		(2) X-rays		
				(3) collect blood		
				(4) micro-CT		
				(5) histology		
rats – Sprague–Dawley	stainless steel in femur	*S. aureus* ATCC 29213	1 week	(1) collect blood	model of effect of ethylenediaminetetraacetic acid to decrease implant infection	180
		1×10^7 CFU		(2) histology		
		E. coli ATCC 25922				
		1×10^7 CFU				
rats – Sprague–Dawley	none	*S. aureus*	2 weeks	(1) CFU count	^{68}Ga-citrate for PET imaging of implant infections	36

models to establish and study implant infections						
animal model	**implant/location**	**pathogen**	**study duration**	**key evaluation**	**summary**	**ref**
		3×10^8 CFU		(2) peripheral quantitative computed tomography		
				(3) histology		
				(4) ^{68}Ga-citrate-chloride PET/CT imaging		
rats – Wistar	poly(ether ether ketone) in tibia	*S. epidermidis* Epi103.1	4 weeks	(1) CFU count	longitudinal micro-CT imaging of implant infection with aerobic and anaerobic pathogens	116
		1×10^6 CFU		(2) time lapse micro-CT		
		P. acnes Type IA, IB				
		1×10^6 CFU				
rats – Wistar	poly(ether ether ketone) and titanium in tibia	*S. aureus* JAR 06.01.31	4 weeks	(1) CFU count	model of morphological bone changes near infected implant	117
		3×10^7 CFU		(2) *in vivo* micro-CT		
				(3) histology		
				(4) pull-out testing		
rabbits – New Zealand White	3D printed stainless steel + PMMA in tibia	*S. aureus* ATCC 29213	1 week	(1) CFU counts	3D printed custom implant for animal models, improve recovery	34
		5×10^6 CFU		(2) collect blood		
				(3) erythrocyte sedimentation rate		
rabbits – New Zealand White	3D printed stainless steel + PMMA in tibia	*S. aureus* ATCC 29213	1 week	(1) gait analysis	3D printed custom implant for animal models–improve recovery	134
		5×10^6 CFU		(2) crystal violet biofilm stain on implant		
rabbits – New Zealand White	stainless steel in femur	*S. aureus* ATCC 25923	3 weeks	(1) X-rays	model of implant infection following open fracture	181
		1×10^6 CFU		(2) micro-CT		
				(3) SEM biofilm		
				(4) histology		
rabbits – New Zealand White	TiAl6V4 in tibia	*S. aureus* ATCC 49230	6 weeks	(1) CFU count	model of early implant infections in rabbits	182
		4×10^5 CFU		(2) X-rays		
				(3) histology		

models to establish and study implant infections						
animal model	**implant/location**	**pathogen**	**study duration**	**key evaluation**	**summary**	**ref**
rabbits – New Zealand White	stainless steel in tibia	*P. acnes* 3×10^7 CFU	4 weeks	(1) CFU count (2) collect blood (3) histology	model of anaerobic species implant infection	183
pigs – Danish Landrace	stainless steel in tibia	*S. aureus* 4F9 (porcine) 1×10^2–1×10^4 CFU	5 days	(1) collect blood (2) CT imaging	low-inoculum porcine model of implant infection	184
pigs – Yorkshire-Landrace cross	none	*S. aureus* UAMS-1 1×10^4 CFU	11 and 15 days	(1) CFU count (2) collect blood (3) CT (4) histology	pig model of hematogenous infection	185

Table 6.

Summary of Preclinical *In Vivo* Models from the Past Decade Used to Evaluate the Antimicrobial Activity and Properties of Implanted Biomaterials for Orthopedic Implant-Associated Infection Applications

models to evaluate antimicrobial activity/properties of implanted materials							
animal model	**implant/location**	**pathogen**	**antimicrobial agent**	**study duration**	**key evaluation**	**summary**	**ref**
mice – BALB/C	magnesium in subcutaneous pouch	*P. aeruginosa* PAO1 CTX::lux	none	8 days	(1) CFU count	degradable magnesium implant to modulate host immune response	59
					(2) histology		
					(3) *in vivo* BLI		
					(4) SEM biofilm		
mice – BALB/C	polyester-poly urethane in subcutaneous pouch	*S. aureus* Xen 29	levofloxacin (local, sustained)	4 weeks	(1) CFU count	antibiotic polymer coatings to prevent implant infections	87
		1×10^6 CFU			(2) activity of residual drug in implant		
mice – BALB/C	polyethylene terephthalate in subcutaneous pouch	*P. aeruginosa* PsAer-9	none	1 week	(1) *in vivo* fluorescence	near-infrared fluorescence probes to image implant inflammation and infection	37
					(2) CFU count		
mice – C57B1/6	PEG hydrogel in femur	*S. aureus* UAMS-1	none	1 and 5 weeks	(1) CFU count	lysostaphin hydrogels to prevent implant infections	120
		1.55×10^8 CFU			(2) micro-CT		
		S. aureus USA 300			(3) histology		
		3.43×10^8 CFU					
mice – C57B1/6	none	MRSA USA 300 1×10^6 CFU	None	2 weeks	(1) micro-CT	poly(propylene sulfide) nanoparticles to prevent implant infections	198
					(2) histology		
					(3) *in vivo* BLI		
rats – Sprague–Dawley	chitosan sponge in subcutaneous pouch	none	vancomycin, ciprofloxacin, cefuroxime (local, sustained)	6 weeks	(1) collect blood	degradable antibiotic chitosan sponges to prevent implant infections	83
					(2) HPLC detect drug in plasma		
					(3) *in vivo* degradation		
					(4) tissue drug concentration		

models to evaluate antimicrobial activity/properties of implanted materials

animal model	implant/location	pathogen	antimicrobial agent	study duration	key evaluation	summary	ref
rats – Sprague–Dawley	micropatterned silicone in subcutaneous pouch	*S. aureus* ATCC 6538 1×10^4 CFU	none	<1 week	(1) CFU count	micropatterned implant to prevent implant infection	41
rats – Sprague–Dawley	silicone in subcutaneous pouch	*S. aureus* ATCC 29213 1×10^8 CFU	none	1–2 weeks	(1) CFU count (2) SEM biofilm (3) histology	nitric oxide releasing implant coatings to prevent implant infection	135
rats – Sprague–Dawley	silver hydroxyapatite coated titanium in subcutaneous pouch	MRSA UOEH6 10×10^8 CFU	none	1 week	(1) quantify biofilm	composite implant coating to mitigate biofilm	148
rats – Sprague–Dawley	Eudragit particle coated Ti6Al4V in subcutaneous pouch	none	vancomycin (local, sustained)	1 week	(1) collect blood (2) LC-MS detect drug in serum	antibiotic coated implant to prevent infection	161
rats – Wistar	hydroxyapatite/calcium sulfate in subcutaneous pouch	none	rifampin (local, sustained)	4 weeks	(1) collect blood (2) HPLC detect drug in serum and bone	antibiotic bioactive ceramic for treating implant infections	144
rats – Wistar	titanium in tibia	none	none	1–4 weeks	(1) histology (2) X-rays (3) forced swimming test	hydroxyapatite and metal coating for promoting implant osseointegration	147
rats – Wistar	stainless steel in femur	*S. aureus* ATCC 29213 1×10^8 CFU	vancomycin, moxifloxacin (systemic)	3 weeks	(1) collect blood (2) HPLC detect drug in serum (3) minimum inhibitory concentration drugs	evaluation of tissue concentration of antibiotics for prevention of implant infection	196
rabbits – New Zealand White	Ti6Al4V in femur	*P. aeruginosa* Pa11 1×10^6 CFU	none	5 weeks	(1) CFU count (2) X-rays (3) histology	method to detect presence of implant infection through urine with biomaterials	40

models to evaluate antimicrobial activity/properties of implanted materials							
animal model	**implant/location**	**pathogen**	**antimicrobial agent**	**study duration**	**key evaluation**	**summary**	**ref**
					(4) micro-CT		
					(5) measure Al in urine		
rabbits – New Zealand White	calcium sulfate in tibia	none	gentamicin, vancomycin, tobramycin (local, sustained)	4–12 weeks	(1) X-rays	calcium sulfate to promote osseointegration of implants	141
					(2) micro-CT		
					(3) histology		
rabbits – New Zealand White	calcium sulfate in tibia	none	vancomycin (local, sustained)	4 weeks	(1) collect blood	calcium sulfate with bone morphogenic protein-2 to promote osseointegration and prevent implant infection	143
					(2) HPLC detect drug in serum and bone		
					(3) histology		
rabbits – New Zealand White	calcium sulfate in tibia	none	gentamicin, vancomycin, tobramycin (local, sustained)	4 weeks	(1) X-rays	antibiotic calcium sulfate to prevent implant infection	142
					(2) collect blood		
					(3) HPLC detect drug in serum and bone		
rabbits – New Zealand White	calcium phosphate granules in tibia	MRSA clinical	vancomycin, tobramycin (local, sustained)	4 weeks infection	(1) CFU count	biodegradable antibiotic cement for treatment of MRSA implant infection	197
		5×10^7 CFU		6 weeks antibiotics	(2) X-rays		
					(3) SEM		
					(4) histology		
					(5) HPLC detect drug		

ACS Infect Dis. Author manuscript; available in PMC 2022 November 28.

Table 7.

Summary of Preclinical *In Vivo* Models from the Past Decade Used to Evaluate the Prevention of Orthopedic Implant-Associated Infections with Antimicrobial Biomaterials

models to evaluate prevention of implant-associated infections							
animal model	**implant/location**	**pathogen**	**antimicrobial agent**	**study duration**	**key evaluation**	**summary**	**reference**
mice – BALB/C	titanium in femur	*S. aureus* Xen 29	none	4 weeks	(1) collect blood	hydroxyapatite coating with ionic silver to prevent implant infections	186, 187
		1×10^8 CFU			(2) *in vivo* BLI		
					(3) histology		
mice – BALB/C	stainless steel in femur	MRSA ATCC 43300	linezolid and MR-5 bacteriophage (local, sustained)	3 weeks	(1) CFU count	antibiotic and bacteriophage implant coatings for infection prevention	221
		1×10^5–1×10^8 CFU			(2) gait analysis		
					(3) histology		
					(4) X-rays		
mice – BALB/C	titanium in femur	*S. aureus* ATCC 25923	none	2 weeks	(1) SEM biofilm	nanocomposite tantalum oxynitride-silver coating to prevent implant infection	222
		5×10^5 CFU					
mice – BALB/C	silicon nitride in tibia	MRSA USA 300	none	2 weeks	(1) SEM biofilm	role of surface topography of silicon nitride to prevent implant infection	38
		1×10^5 CFU			(2) histology		
mice – C57Bl/6	stainless steel tibia	*S. aureus* ATCC 43300	none	2 weeks	(1) micro-CT	aspirin to facilitate healing of implant infections	223
		1×10^6 CFU			(2) histology		
mice – C57Bl/6	stainless steel in L4 spine and femur	*S. aureus* Xen 36	vancomycin, tigecycline (local, sustained)	4 and 6 weeks	(1) CFU count	PEG-poly(propylene sulfide) coating to prevent implant infections	90–92
		1×10^3 CFU			(2) *in vivo* BLI		
					(3) X-rays		
mice – C57Bl/6	stainless steel or titanium in femur	*S. aureus* Xen 36	vancomycin, daptomycin, tigecycline (systemic)	1 week	(1) CFU count	model to compare efficacy of prophylactic antibiotics for implant infections	188
		1×10^4 CFU			(2) X-rays		
					(3) *in vivo* BLI		

models to evaluate prevention of implant-associated infections

animal model	implant/location	pathogen	antimicrobial agent	study duration	key evaluation	summary	reference
					(4) SEM biofilm		
mice – Lys-EGFP	stainless steel in femur	*S. aureus* ALC-2906	rifampin, minocycline (local, sustained)	2 weeks	(1) CFU counts	antibiotic polyesteramide coating to prevent implant infections	93
		5×10^2 CFU			(2) *in vivo* BLI		
					(3) histology		
					(4) SEM biofilm		
mice – Kunming	titanium in femur	MRSA USA 300	none	4 weeks	(1) CFU count	graphdiyne-titanium oxide nanofiber composite implant prevent implant infections	224
		1×10^7 CFU			(2) histology		
					(3) SEM		
rats – Sprague–Dawley	stainless steel in tibia	*S. aureus* ATCC 49230	gentamicin (local, sustained)	6 weeks	(1) CFU count	gentamicin in poly(D-L-lactide) coating to prevent implant infections	94–96
		1×10^2– 1×10^3 CFU			(2) collect blood		
					(3) X-rays		
					(4) histology		
rats – Sprague–Dawley	titanium in femur	*S. aureus* ATCC 25923	none	6 weeks	(1) micro-CT	dimethylaminododecyl methacrylate and hydroxyapatite coated implant to prevent infection and promote osteogenesis	225
		1×10^8 CFU			(2) histology		
					(3) biocompatibility		
rats – Sprague–Dawley	magnesium and titanium in femur	*MRSA* ATCC 43300	none	8 weeks	(1) CFU count	magnesium to prevent MRSA implant infections	226
		1×10^6 CFU			(2) X-rays		
					(3) micro-CT		
					(4) SEM of biofilms		
rats – Sprague–Dawley	titanium in femur	*S. aureus* ATCC 29213	none	4 weeks	(1) CFU counts	layer-by-layer coating (silver nanoparticles + poly-L-glutamic acid and polyallylamine to prevent implant infection	227
		1×10^6 CFU			(2) micro-CT		
					(3) histology		
rats – Sprague–Dawley	titanium in femur	*S. aureus* ATCC 49230	gentamicin palmitate (local, sustained)	6 weeks	(1) CFU count	antibiotic coated implant for infection prevention	228

models to evaluate prevention of implant-associated infections							
animal model	**implant/location**	**pathogen**	**antimicrobial agent**	**study duration**	**key evaluation**	**summary**	**reference**
		1×10^2 CFU			(2) X-rays		
					(3) collect blood		
					(4) histology		
rats – Sprague–Dawley	TiAl6V4 in tibia	*S. aureus* ATCC 49230	gentamicin (local, sustained)	4 weeks	(1) CFU count	antibiotic coated titanium oxide implant for infection prevention and osseointegration	229
		1×10^4 CFU			(2) X-rays		
					(3) histology		
rats – Sprague–Dawley	titanium in femur	*S. aureus* ATCC 25923	none	1–12 weeks	(1) CFU count	poly(glycidyl methacrylate) and quaternized poly (ethylene imine) functionalized titanium implants with alendronate for infection prevention and osseointegration	122
		1×10^9 CFU			(2) micro-CT		
					(3) histology		
					(4) pull-out test		
rats – Sprague–Dawley	titanium in tibia	*S. aureus* ATCC 25923	none	4 weeks	(1) CFU count	poly-L-lysine functionalized implants for infection prevention and osseointegration	230
		1×10^4 CFU			(2) micro-CT		
					(3) histology		
rats – Sprague–Dawley	titanium in femur	*S. aureus* ATCC 25923	gentamicin (local, sustained)	6 weeks	(1) CFU count	antibiotic nanotube implants for infection prevention and osseointegration	231
		1×10^5 CFU			(2) X-rays		
					(3) histology		
rats – Sprague–Dawley	poly(ether ether ketone) in tibia	*S. aureus* Xen 29	gentamicin (local, sustained)	1–8 weeks	(1) CFU count	nanolayered antibiotic and bone morphogenic protein-2 implant coating for infection prevention and osseointegration	97
		5×10^5 CFU			(2) micro-CT		
					(3) histology		
					(4) pull-out testing		
rats – Sprague–Dawley	titanium in femur	*S. aureus* ATCC 29213	none	1 week	(1) CFU count	hydrophobic triethoxysilane implant coating for infection prevention	232
		1×10^6 CFU			(2) histology		
rats – Sprague–Dawley	PMMA in femur	MRSA clinical	teicoplanin (local, sustained)	3 weeks	(1) CFU count	antibiotic and calcium sulfate PMMA to prevent implant infections	129
		1×10^8 CFU			(2) X-rays		

models to evaluate prevention of implant-associated infections							
animal model	**implant/location**	**pathogen**	**antimicrobial agent**	**study duration**	**key evaluation**	**summary**	**reference**
					(3) histology		
rats – Sprague–Dawley	stainless steel in femur	*S. aureus* ATCC 43300	none	6 weeks	(1) micro-CT	sodium butyrate modified implant to mitigate infection and promote osteogenesis	112
		1×10^4 CFU			(2) histology		
rats – Sprague–Dawley	copper-poly(ether ether ketone) in femur	MRSA ATCC 43300	none	4 weeks	(1) CFU count	composite implant to prevent MRSA infection	114
		1×10^6 CFU			(2) micro-CT		
					(3) histology		
					(4) biocompatibility		
rats – Sprague–Dawley	poly(ether ether ketone) in femur	*S. aureus* ATCC 6538	gentamicin (local, sustained)	4–6 weeks	(1) X-rays	antibiotic composite implant to promote osseointegration and prevent infection	113
		1×10^4 CFU			(2) micro-CT		
					(3) histology		
rats – Sprague–Dawley	gallium–strontium magnesium alloy in femur	*S. aureus* ATCC 43300	none	5 days	(1) CFU count	metal alloys for intrinsic prevention of implant infections	233
		1×10^5 CFU			(2) histology		
					(3) SEM		
rats – Sprague–Dawley	Pro Osteon 500R + PEG + poly (capro-lactone) + PLGA in tibia	*S. aureus* ATCC 49230	rifampin, vancomycin (local, sustained)	10 weeks	(1) CFU count	antibiotic putty to prevent implant infection	98
		1×10^8 CFU			(2) X-rays		
					(3) micro-CT		
					(4) histology		
rats – Sprague–Dawley	3D printed titanium in tibia	*S. aureus* ATCC 49230	vancomycin (local, sustained)	4 weeks	(1) CFU count	chitosan silver particle antibiotic implant coatings to prevent infection	99
		1×10^6 CFU			(2) micro-CT		
					(3) collect blood		
					(4) histology		
rats – Wistar	titanium in femur	*S. aureus* Xen 40	none	6 weeks	(1) CFU count	vitamin E phosphate coating to improve implant integration	189
		3×10^4 CFU			(2) collect blood		

models to evaluate prevention of implant-associated infections							
animal model	**implant/location**	**pathogen**	**antimicrobial agent**	**study duration**	**key evaluation**	**summary**	**reference**
					(3) micro-CT		
					(4) histology		
					(5) *in vivo* BLI		
rats – Wistar	Ti6Al4V in tibia	*S. aureus* ATCC 25923	none	6 weeks	(1) CFU count	hydroxyapatite and silver coated implant infection model	234
		1×10^2–1×10^3 CFU			(2) X-rays		
					(3) histology		
rabbits – Dutch Belted	titanium in femur	*S. aureus* SAP231	linezolid, rifampin (local, sustained)	1 week	(1) CFU count	PLGA and poly(caprolactone) nanofiber coated implant infection model	100
		1×10^4 CFU			(2) *in vivo* BLI		
rabbits – New Zealand White	stainless steel in tibia	MRSA ATCC 43300	none	6 weeks	(1) micro-CT	titanium with nanothick calcium oxide MRSA implant infection model	246
		1×10^4 CFU			(2) histology		
rabbits – New Zealand White	titanium in femur	MRSA ATCC 43300	none	6 weeks	(1) CFU count	silver ion calcium phosphate ceramic nanopowder implant coating infection model	150
		5×10^2 CFU			(2) X-rays		
					(3) histology		
rabbits – New Zealand White	Porous tantalum in radius	*S. aureus* ATCC 49230	tobramycin (local, sustained)	2 weeks	(1) X-rays	antibiotic PLGA microspheres in porous implant to prevent infections	101
		2×10^6 CFU			(2) histology		
rabbits – New Zealand White	titanium in tibia	*S. aureus* ATCC 10832	tobramycin (local, sustained)	4 weeks	(1) CFU count	antibiotic-periapatite coated implants to prevent infection and promote osseointegration	236
		1×10^3–1×10^5 CFU			(2) collect blood		
					(3) histology		
					(4) erythrocyte sedimentation rate		
rabbits – New Zealand White	stainless steel in humerus	*S. aureus* JAR 060131	gentamicin (local, sustained)	1 week	(1) CFU count	injectable antibiotic thermoresponsive hyaluronic acid implant coating to prevent infections	23
		2×10^6 CFU			(2) X-rays		
					(3) collect blood		
					(4) histology		

models to evaluate prevention of implant-associated infections

animal model	implant/location	pathogen	antimicrobial agent	study duration	key evaluation	summary	reference
rabbits – New Zealand White	titanium and stainless steel in humerus	*S. aureus* JAR 060131	none	4 weeks	(1) CFU count	impact of implant topography on infection prevention	237
		2×10^3–2×10^5 CFU			(2) X-rays		
rabbits – New Zealand White	titanium in femur	MRSA clinical isolate	vancomycin (local, sustained)	12 weeks	(1) CFU count	antibiotic hydrogel implant coating for infection prevention	102
		5×10^4–5×10^6 CFU			(2) collect blood		
					(3) histology		
rabbits – New Zealand White	titanium in femur	*S. aureus* ATCC 6538P	none	1 week	(1) CFU count	antimicrobial fusion peptide implant coating for infection prevention and osseointegration	238
		1×10^8 CFU			(2) micro-CT		
					(3) histology		
rabbits – New Zealand White	titanium in tibia	*S. aureus* ATCC 25923	none	4 weeks	(1) CFU count	molybdenum disulfide/polydopamine – RGD implant coating for infection prevention	239
		2×10^3 CFU			(2) micro-CT		
					(3) histology		
rabbits – New Zealand White	Ti6Al4V in femur	MRSA ATCC 43300	none	10 weeks	(1) CFU count	silver and ceramic implant coating for infection prevention	157
		5×10^4 CFU			(2) collect blood		
					(3) histology		
rabbits – New Zealand White	magnetic iron oxide particles with carbon nanotubes in tibia	MRSA CCTCC 16465	gentamicin (local, sustained)	2 weeks	(1) CFU count	bacterial capturing implant infections with magnetic microwave activated composites	26
		1×10^6 CFU			(2) collect blood		
					(3) histology		
					(4) MRI		
rabbits – New Zealand White	calcium phosphate in tibia	*S. aureus* Xen 29	tobramycin (local, sustained)	4 weeks	(1) CFU count	antibiotic calcium phosphate for prevention of implant infections	190
		1×10^7 CFU			(2) collect blood		
					(3) X-rays		
					(4) histology		
rabbits – New Zealand White	chitosan and calcium phosphate in tibia	*S. aureus*	moxifloxacin (local, sustained)	4 weeks	(1) CFU count	composite antibiotic material for prevention of implant infection	240
		1×10^6 CFU			(2) histology		

models to evaluate prevention of implant-associated infections							
animal model	**implant/location**	**pathogen**	**antimicrobial agent**	**study duration**	**key evaluation**	**summary**	**reference**
sheep	stainless steel in tibia	*S. aureus* ATCC 6538	cefazolin (local, sustained)	7 days	(1) CFU count	antibiotic filled steel implants for infection prevention in sheep	241, 242
		6.6×10^6 CFU			(2) collect blood		
					(3) histology		
					(4) antibiotic distribution		
sheep – Rambouillet	titanium in femur	MRSA clinical	trialkyl norspermidine-biaryl (local, sustained)	4 and 24 weeks	(1) CFU count	antimicrobial compound active release implant coating for infection prevention	243
		2×10^8 CFU			(2) X-rays		
					(3) SEM		
					(4) histology		
sheep – Columbia Cross	hydroxyapatite calcium carbonate and PLGA in femur	*S. aureus* ATCC 49230	tobramycin (local, sustained)	12 weeks	(1) CFU count	antibiotic bone void filler to prevent implant infection	103
		5×10^5 CFU			(2) collect blood		
					(3) micro-CT		
					(4) histology		
sheep – Dorset Cross	titanium plate in tibia	*S. aureus* ATCC 25923	vancomycin (local, sustained)	12 weeks	(1) CFU count	antibiotic modified implant surface to prevent infection	244
		2×10^6 CFU			(2) X-rays		
					(3) SEM biofilm		
					(4) histology		
					(5) gait analysis		
sheep – English Mule	PLGA and PEG in femur	*S. aureus* F2789	gentamicin, clindamycin (local, sustained)	2 and 13 weeks	(1) CFU count	injectable and biodegradable antibiotic gel to prevent implant infection	104
		2×10^6 CFU			(2) collect blood		
					(3) micro-CT		
					(4) histology		
goat	stainless steel in tibia	*S. aureus* ATCC 25923	none	5 weeks	(1) X-rays	titanium oxide and siloxane implant coating to prevent infection	245
		2×10^4 CFU			(2) micro-CT		

models to evaluate prevention of implant-associated infections							
animal model	**implant/location**	**pathogen**	**antimicrobial agent**	**study duration**	**key evaluation**	**summary**	**reference**
					(3) histology (4) silver and titanium in organs		
goat – Spanish	PMMA and calcium sulfate in tibia	*S. aureus* ATCC 29213 2×10^6 CFU	tobramycin (local, sustained)	3 weeks	(1) CFU count	evaluation of ability of commercial antibiotic composites for prevention of implant infection	130

Table 8.

Summary of Preclinical *In Vivo* Models from the Past Decade Used to Evaluate the Treatment of Orthopedic Implant-Associated Infections with Antimicrobial Agents and Biomaterials

models to evaluate treatment of implant-associated infections							
animal model	**implant/location**	**pathogen**	**antimicrobial agent**	**study duration**	**key evaluation**	**summary**	**ref**
mice – BALB/C	titanium in femur	*S. aureusATCC*	gentamicin, vancomycin (local, sustained)	6 weeks	(1) CFU counts	antibiotic calcium sulfate/ hydroxyapatite spacer for infection treatment	247
		292131.35 × 10^5 CFU			(2) collect blood		
					(3) X-rays		
mice – BALB/C	poly(ether ether ketone) and titanium in femur	*S. aureus* Xen 36	vancomycin, rifampin (local, sustained)	1 week infection	(1) CFU count	3D printed calcium phosphate and PMMA antibiotic spacers for infection treatment	118
		8 × 10^4 CFU		3 weeks antibiotics	(2) *in vivo* BLI		
					(3) X-rays		
					(4) micro-CT		
					(5) SEM biofilm		
mice – BALB/C	poly(ether ether ketone) and titanium in femur	*S. aureus* Xen 36	vancomycin (local, sustained)	1 week infection	(1) CFU count	antibiotic PMMA spacers for infection treatment	119
		8 × 10^4 CFU		3 weeks antibiotics	(2) *in vivo* BLI		
					(3) micro-CT		
mice – BALB/C	titanium in femur	*S. aureus* Xen 36	gentamicin (local, sustained)	1 week infection	(1) CFU count	antibiotic PMMA spacers for infection treatment	126
		2.5 × 10^6 CFU		2 weeks antibiotics	(2) X-rays		
					(3) *in vivo* BLI		
mice – BALB/C	stainless steel in tibia	*S. aureus* UAMS-1	cefazoline, gentamicin, vancomycin, rifampin (systemic)	1 week infection	(1) CFU count	evaluation of combination antibiotics for treatment of implant biofilms	248
		2.5 × 10^5 CFU		2 weeks antibiotics	(2) SEM biofilm		
					(3) histology		
mice – C57Bl/6	titanium in femur	MRSA USA 300	linezolid, rifampin, vancomycin, daptomycin (systemic)	2 weeks infection	(1) CFU count	evaluation of combination antibiotics for treatment of implant infection	249
		1 × 10^3 CFU		6 weeks antibiotics	(2) *in vivo* BLI		

models to evaluate treatment of implant-associated infections							
animal model	**implant/location**	**pathogen**	**antimicrobial agent**	**study duration**	**key evaluation**	**summary**	**ref**
					(3) X-rays		
					(4) micro-CT		
mice – C57Bl/6	titanium in tibia	*S. aureus* Xen 36	vancomycin (local, sustained)	2 weeks infection	(1) CFU count	antibiotic PMMA spacers for infection treatment, need for intravenous antibiotics	127
		3×10^5 CFU		4 weeks antibiotics	(2) collect blood		
					(3) X-rays		
rats – Sprague–Dawley	Kirschner wire in tibia	*MRSA* 40496/08	dalbavancin, vancomycin (systemic)	4 weeks	(1) CFU count	antibiotics for implant MRSA infection treatment	250
		$1–5 \times 10^6$ CFU			(2) X-rays		
rats – Sprague–Dawley	intramedullary implant in tibia	*S. aureus* EDCC 5055	none	6 weeks	(1) CFU count	use of CpG oligodeoxynucleotide to treat implant infections	251
		1×10^3 CFU			(2) histology		
rats – Sprague–Dawley	Kirschner wire in tibia	MRSA N315	vancomycin (local, sustained)	2 weeks infection	(1) CFU count	antibiotic silicone cement for treatment of implant infection	260
		1×10^8 CFU		4 weeks antibiotics	(2) X-rays		
					(3) histology		
rats – Sprague–Dawley	PMMA in tibia	MRSA ATCC 25923	fusidic acid (local, sustained), teicoplanin (systemic)	3 weeks infection	(1) CFU count	antibiotic cement with systemic antibiotics for treatment of implant infection	131
		5×10^5 CFU		2 weeks antibiotics	(2) histology		
rats – Sprague–Dawley	alginate-hyaluronic acid in femur	*S. aureus* KCTC1621	vancomycin (local, sustained)	2 weeks infection	(1) CFU count	*in situ* gelling hydrogel for treatment of implant infections	85
		1×10^4 CFU		3 and 6 weeks antibiotics	(2) micro-CT		
					(3) collect blood		
					(4) X-rays		
rats – Sprague–Dawley	injectable alginate hydrogel in femur	*S. aureus* ATCC 6538	fosfomycin (local, sustained)	1 week infection	(1) CFU count	injectable antibiotic hydrogel and bacteriophage for treatment of implant infections	105
		5×10^4 CFU		1 week antibiotics	(2) SEM		
					(3) histology		

models to evaluate treatment of implant-associated infections

animal model	implant/location	pathogen	antimicrobial agent	study duration	key evaluation	summary	ref
rats – Sprague–Dawley	silver nanoparticles in gelatin sponge in tibia	MRSA ATCC 43300	teicoplanin (local sustained)	3 weeks infection	(1) X-ray	silver nanoparticles for treatment of implant infections	252
		1×10^7 CFU		3 weeks antibiotics	(2) collect blood		
rats – Wistar	stainless steel in femur	*S. aureus* ATCC 29213	moxifloxacin, flucloxacillin, rifampin, vancomycin (systemic)	1 week infection	(1) CFU count	evaluation of combination antibiotics for treatment of implant infection	253, 254
		1×10^8 CFU		2 weeks antibiotics			
rats – Wistar	collagen sponge and PMMA beads in tibia	*S. aureus* ATCC 292113	gentamicin, cefazolin (local, sustained)	3 weeks infection	(1) CFU count	comparison of antibiotic carrier for treatment of implant infections	86
		5×10^6 CFU		2 or 4 weeks antibiotics			
rats – Wistar	poly(D-L-lactide-*co*-glycolide-*co*-ε-capro-lactone) in tibia	*S. aureus*	ciprofloxacin (local, sustained)	4 weeks infection	(1) CFU count	antibiotic poly(D-L-lactide-*co*-glycolide-*co*-ε-caprolactone) implant coating to treat infections	255
		1×10^8 CFU		4 weeks antibiotics	(2) collect blood		
rats – Wistar	magnetite encapsulated gelatin particles in tail vein	*S. aureus*	gentamicin (local, sustained)	2 weeks infection	(1) X-rays	magnetite antibiotic particles for treatment of implant infection	25
		1×10^9 CFU		2 weeks antibiotic	(2) collect blood		
					(3) histology		
rats – Long-Evans	titanium in humerus	MRSA NR0	vancomycin (systemic)	6 day infection	(1) CFU count	electrical stimulation with antibiotics to treat implant infection	27
		1×10^5 CFU		5 weeks antibiotics	(2) X-rays		
					(3) histology		
rabbits – New Zealand White	silicone elastomer in tibia	MRSA S271 ST20121238	daptomycin, rifampin, ceftaroline (systemic)	1 week infection	(1) CFU count	evaluation of combination antibiotics for treatment of MRSA implant infection	256, 257
		5×10^7 CFU		10 days antibiotics			
rabbits – New Zealand White	stainless steel in tibia	MRSA EDCC 5443 EDCC 5398	vancomycin (local, sustained)	4 weeks infection	(1) CFU count	antibiotic PMMA spacer for two-stage implant infection revision	132
		1×10^5–1×10^7 CFU		4 weeks antibiotics	(2) X-rays		
					(3) histology		

models to evaluate treatment of implant-associated infections

animal model	implant/location	pathogen	antimicrobial agent	study duration	key evaluation	summary	ref
rabbits – New Zealand White	Ti6Al4 V in femur	*S. aureus* ATCC 29213	gentamicin (local, sustained)	1 week infection	(1) CFU count	antibiotic PMMA chain for treatment of implant infection (copper and titanium oxide coated)	133
		1×10^5 CFU		2 weeks antibiotics	(2) collect blood		
rabbits – New Zealand White	borate bioactive glass in tibia	MRSA ATCC 43300	vancomycin (local, sustained)	8 weeks	(1) CFU count	injectable borate bioactive glass for treating implant infection	30
		1×10^8 CFU			(2) collect blood		
					(3) X-rays		
					(4) histology		
rabbits – New Zealand White	calcium sulfate in tibia	*S. aureus* ATCC 29213	gentamicin (local, sustained)	2 weeks infection	(1) CFU count	antibiotic calcium sulfate to treat implant infection	28
		2×10^6 CFU		2 weeks antibiotics	(2) X-rays		
					(3) collect blood		
rabbits – New Zealand White	PLGA in femur	*S. aureus* ATCC 65389	vancomycin (local, sustained)	2 weeks infection	(1) CFU count	monitor treatment of implant infections with ^{18}F-FDG-PET imaging	35
		1×10^5 CFU		2 weeks antibiotics	(2) ^{18}F-FDG-PET imaging		
rabbits – New Zealand White	Hydroxyapatite–polyamino acid in tibia	*S. aureus*	vancomycin (local, sustained)	2 weeks infection	(1) CFU counts	antibiotic hydroxyapatite/polyamino acid for treatment of implant infection and osteogenesis	235
		1×10^8 CFU		6 weeks antibiotics	(2) X-ray		
					(3) collect blood		
					(4) histology		
rabbits – New Zealand White	stainless steel with silver particles in femur	*S. aureus* ATCC 29213	none	3 weeks infection	(1) CFU count	silver nanoparticle implant coating to treat infections	258
		3×10^6 CFU		3 weeks treatment	(2) X-rays		
					(3) histology		
					(4) SEM		
rabbits – New Zealand White	Hydroxyapatite–polyamino acid PLGA in tibia	*S. aureus* ATCC 25923	rifapentine (local, sustained)	4 weeks infection	(1) CFU count	antibiotic composite material for treatment of implant infection	106
		3×10^8 CFU		4 weeks antibiotics	(2) collect blood		
					(3) X-rays		

models to evaluate treatment of implant-associated infections							
animal model	**implant/location**	**pathogen**	**antimicrobial agent**	**study duration**	**key evaluation**	**summary**	**ref**
					(4) histology		
					(5) gait analysis		
rabbits – New Zealand White	chitosan thermosensitive hydrogel in tibia	*S. aureus* Kanin	vancomycin (local, sustained)	4 weeks infection	(1) collect blood	injectable thermosensitive hydrogel with quaternary ammonium chitosan for treatment of implant infections	24
		1×10^8 CFU		4–8 weeks antibiotics	(2) micro-CT		
					(3) histology		
dogs – Beagle	stainless steel in femur	*S. aureus* ATCC 29213	ciprofloxacin (local, sustained)	4 weeks infection	(1) CFU count	amylose starch antibiotic coated implants to treat infection	259
		3×10^8 CFU		6 weeks antibiotics	(2) X-rays		
					(3) histology		